Cholesterol transport from late endosomes to the Golgi regulates t-SNARE trafficking, assembly, and function

Meritxell Reverter[a], Carles Rentero[a], Sandra Vilà de Muga[a], Anna Alvarez-Guaita[a], Vishwaroop Mulay[b], Rose Cairns[b], Peta Wood[b], Katia Monastyrskaya[c], Albert Pol[a,d,e], Francesc Tebar[a], Joan Blasi[f], Thomas Grewal[b], and Carlos Enrich[a,d]

[a]Departament de Biologia Cel·lular, Immunologia i Neurociències, Facultat de Medicina, Universitat de Barcelona, 08036 Barcelona, Spain; [b]Faculty of Pharmacy, University of Sydney, Sydney, NSW 2006, Australia; [c]Urology Research Laboratory, Department of Clinical Research, University of Bern, 3000 Bern 9, Switzerland; [d]Institut d'Investigacions Biomèdiques August Pi i Sunyer (IDIBAPS), Facultat de Medicina, Universitat de Barcelona, 08036 Barcelona, Spain; [e]Institució Catalana de Recerca i Estudis Avançats (ICREA), 08010 Barcelona, Spain; [f]Department of Pathology and Experimental Therapeutics, IDIBELL–University of Barcelona, 08907 L'Hospitalet de Llobregat, Barcelona, Spain

ABSTRACT **Cholesterol regulates plasma membrane (PM) association and functioning of syntaxin-4 and soluble *N*-ethylmaleimide-sensitive fusion protein 23 (SNAP23) in the secretory pathway. However, the molecular mechanism and cellular cholesterol pools that determine the localization and assembly of these target membrane SNAP receptors (t-SNAREs) are largely unknown. We recently demonstrated that high levels of annexin A6 (AnxA6) induce accumulation of cholesterol in late endosomes, thereby reducing cholesterol in the Golgi and PM. This leads to an impaired supply of cholesterol needed for cytosolic phospholipase A_2 ($cPLA_2$) to drive Golgi vesiculation and caveolin transport to the cell surface. Using AnxA6-overexpressing cells as a model for cellular cholesterol imbalance, we identify impaired cholesterol egress from late endosomes and diminution of Golgi cholesterol as correlating with the sequestration of SNAP23/syntaxin-4 in Golgi membranes. Pharmacological accumulation of late endosomal cholesterol and $cPLA_2$ inhibition induces a similar phenotype in control cells with low AnxA6 levels. Ectopic expression of Niemann-Pick C1 (NPC1) or exogenous cholesterol restores the location of SNAP23 and syntaxin-4 within the PM. Importantly, AnxA6-mediated mislocalization of these t-SNAREs correlates with reduced secretion of cargo via the SNAP23/syntaxin-4–dependent constitutive exocytic pathway. We thus conclude that inhibition of late endosomal export and Golgi cholesterol depletion modulate t-SNARE localization and functioning along the exocytic pathway.**

Monitoring Editor
Jean E. Gruenberg
University of Geneva

Received: Apr 19, 2011
Revised: Aug 11, 2011
Accepted: Aug 26, 2011

This article was published online ahead of print in MBoC in Press (http://www.molbiolcell.org/cgi/doi/10.1091/mbc.E11-04-0332) on September 7, 2011.

Address correspondence to: Carlos Enrich (enrich@ub.edu) or Thomas Grewal (thomas.grewal@sydney.edu.au).

Abbreviations used: A431wt, A431 wild-type; AA, arachidonic acid; Anx, annexin; CD, methyl-β-cyclodextrin; CHOwt, CHO wild-type; $cPLA_2$, cytosolic phospholipase A2; DRM, detergent resistant membranes; EGFP, enhanced green fluorescent protein; ELISA, enzyme-linked immunosorbent assay; FN, fibronectin; GFP, green fluorescent protein; LDL, low-density lipoprotein; LDM, low-density membrane; ; LPS, lipopolysaccharide; MAFP, methyl arachidonyl fluorophosphonate; ManII, mannosidase II; MDCK, Madin-Darby canine kidney; NPC1, Niemann-Pick type C1; NRS, normal rabbit serum; NSF, *N*-ethylmaleimide-sensitive factor; ORP, OSBP-related protein; OSBP, oxysterol-binding protein; PM, plasma membrane; PMSF, phenylmethylsulfonyl fluoride; PUFA, polyunsaturated fatty acid; RPMI, Roswell Park Memorial Institute medium; SEAP, secreted alkaline phosphatase; SNAP23, synaptosomal-associated protein 23; SNARE, SNAP (soluble NSF attachment protein) receptor protein; START domain, StAR-related lipid transfer domain; STED, stimulated emission depletion; TCS, true confocal scanning; TGN, *trans*-Golgi network; TIRF-M, total internal reflection fluorescence microscopy; TNF-α, tumor necrosis factor α; t-SNARE, target membrane SNARE; U18666A, 3-β-[2-(diethylamino) ethoxy] androst-5-en-17-one; VAMP, vesicle-associated membrane protein; v-SNARE, vesicle membrane SNARE; WCL, whole-cell lysate; YFP, yellow fluorescent protein.

INTRODUCTION

In recent years, the involvement of annexins in membrane recognition and trafficking has emerged as one of their predominant functions (Gerke and Moss, 2002; Gerke *et al.*, 2005; Lemmon, 2008; Grewal *et al.*, 2010; Enrich *et al.*, 2011). Annexins are a family of structurally related Ca^{2+}-regulated membrane-binding proteins. Among the 12 members of the mammalian family, annexins (Anx) A1, A2, A6, A8, and A13b have been particularly implicated in a

variety of intracellular trafficking steps along endo- and exocytic pathways (Fiedler *et al.*, 1995; Mayran *et al.*, 2003; Babiychuk *et al.*, 2008; Goebeler *et al.*, 2008; Grewal and Enrich, 2009; Monastyrskaya *et al.*, 2009a; Morel *et al.*, 2009).

We and others have shown that AnxA6 is a highly dynamic protein involved in a number of cellular events linked to membrane transport. This includes the reorganization of the actin cytoskeleton at the plasma membrane (PM; Monastyrskaya *et al.*, 2009b), the delivery of cholesterol from late endosomes to the Golgi and PM (Cubells *et al.*, 2007), the cholesterol-dependent recruitment of $cPLA_2$ to the Golgi and its involvement in Golgi vesiculation (Cubells *et al.*, 2008), as well as signal transduction events at the cell surface and possibly on endosomes (Grewal and Enrich, 2006; Vila de Muga *et al.*, 2009). On cell activation, AnxA6 is predominantly targeted to the PM. This possibly includes the association of AnxA6 with cholesterol-enriched membrane microdomains (lipid rafts, both caveolae and noncaveolae), although the potential role of AnxA6 in these membrane rafts is still unclear (Schnitzer *et al.*, 1995; Foster *et al.*, 2003). Furthermore, we identified AnxA6 as a major component of rat liver endosomes (Jackle *et al.*, 1994; Pol *et al.*, 1997). These findings correlate with the involvement of AnxA6 in low-density lipoprotein (LDL) receptor–mediated endocytosis (Kamal *et al.*, 1998; Grewal *et al.*, 2000) and the delivery of LDL-containing late endosomes to lysosomes for degradation (Pons *et al.*, 2000). LDL-induced translocation of AnxA6 to late endosomes (Grewal *et al.*, 2000) correlates with the recruitment of AnxA6 to cholesterol-enriched late endosomes, which establishes a connection between AnxA6 and cholesterol (de Diego *et al.*, 2002).

Most relevant for the study presented here, cells expressing high levels of AnxA6 show an accumulation of cholesterol in late endosomes, which leads to reduced cholesterol levels in the Golgi and PM. Consequently, cholesterol-dependent caveolin-1 transport from the Golgi apparatus to the cell surface is inhibited, leading to reduced numbers of caveolae at the cell surface (Cubells *et al.*, 2007). Follow-up studies revealed that reduced cholesterol availability in AnxA6-overexpressing cells perturbs cytosolic phospholipase A2 ($cPLA_2$) translocation to the Golgi, which is required to drive cholesterol-dependent vesiculation events (e.g., caveolin transport) from the Golgi apparatus (Cubells *et al.*, 2008). This indirect role for AnxA6 in the secretory pathway and in membrane microdomain formation at the PM is most likely relevant for a large number of cells and tissues, as high amounts of AnxA6 are commonly found in most mammalian tissues, with the exception of undetectable to low AnxA6 levels in epithelial cells of the small intestine, parathyroid gland, and colon, as well as in several cell and mouse models of cancer (Vila de Muga *et al.*, 2009; Grewal *et al.*, 2010).

A number of studies identified a crucial role for cholesterol in PM localization of members of the SNAP receptor (SNARE) superfamily (Chamberlain *et al.*, 2001; Predescu *et al.*, 2005; Lang, 2007). Soluble *N*-ethylmaleimide-sensitive fusion protein 23 (SNAP23) is a ubiquitously expressed target membrane SNARE (t-SNARE) protein attached to the cytoplasmic leaflet of the PM through five palmitoylation moieties. Like SNAP25 and SNAP29, SNAP23 contains two tandem SNARE motifs separated by a linker region. Syntaxin-4 is another widely expressed t-SNARE anchored at the PM through a transmembrane domain. Syntaxin-4 is localized at the basolateral domain of MDCK cells and is important for polarized trafficking, epithelial polarity, and *trans*-Golgi network (TGN)-to-basolateral trafficking (Lafont *et al.*, 1999). SNAP23 binds to syntaxin-4 in vivo (St-Denis *et al.*, 1999) and is involved in biosynthetic and endocytic recycling and transcytotic pathways to both PM domains of MDCK cells (Leung *et al.*, 1998). Both SNAP23 and syntaxin-4 participate in fusion events along the secretory pathway and interact with different vesicle SNAREs (v-SNAREs), such as vesicle-associated membrane protein (VAMP) 2, 3, 7, or 8, depending on the cell type analyzed, to regulate lysosomal fusion with the PM (Rao *et al.*, 2004), apical fusion in epithelial cells (Low *et al.*, 1998), GLUT4 translocation (Bryant *et al.*, 2002), or tumor necrosis factor α (TNF-α) secretion (Hong, 2005; Kay *et al.*, 2006). Interestingly, syntaxin-4 and SNAP23 concentrate in cholesterol-rich clusters that partially colocalize with caveolin-1 in the basolateral PM of endothelial cells. It was proposed that this spatial organization may be required for efficient and rapid caveolar fusion with the target membrane (Predescu *et al.*, 2005).

Recently another t-SNARE, syntaxin-6, was implicated in cholesterol transport from late endosomes to the TGN (Urano *et al.*, 2008). In addition, syntaxin-6 appears to regulate delivery to the cell surface of microdomain-associated lipids and proteins required for caveolae endocytosis (Choudhury *et al.*, 2006). Thus interfering with either cholesterol export from late endosomes or the functioning of certain syntaxins seems to affect caveolin-1 transport and caveolae formation in a similar manner.

This prompted us to examine how differential levels of AnxA6 and the concomitantly induced alterations of cholesterol levels in late endosomes, Golgi, and PM would impact on the subcellular localization and assembly of a subset of t-SNARE proteins within the secretory pathway. Using AnxA6-overexpressing cells as a model for cellular cholesterol imbalance, we show a mechanistic relationship between late endosomal and Golgi cholesterol, $cPLA_2$ function, and t-SNARE proteins involved in the post-Golgi exocytic pathway. Inhibition of cholesterol egress from late endosomes, followed by Golgi cholesterol depletion and $cPLA_2$ inhibition, is responsible for the disintegration of syntaxin-4 and SNAP23 clusters from cholesterol-enriched PM microdomains. This is associated with the retention of SNAP23 and syntaxin-4, together with caveolin-1, in Golgi membranes and the increased formation of SNAP23/syntaxin-4–containing t-SNARE complexes.

These results are in agreement with our previous findings that AnxA6-induced changes in cellular cholesterol distribution inhibit caveolin-1 transport and suggest that t-SNARE dysfunction contributes to impaired caveolae formation in cells with high AnxA6 levels. Furthermore, current findings highlight the fact that AnxA6-mediated and cholesterol-dependent t-SNARE mislocalization also contribute to an impaired secretion of cargo through SNAP23/syntaxin-4–dependent constitutive exocytosis, and suggest that t-SNARE dysfunction adds to impaired caveolae formation in cells with high AnxA6 levels. The physiological consequences of AnxA6's potential regulation of t-SNARE function via intracellular cholesterol trafficking routes exiting late endosomes are discussed.

RESULTS

As outlined in the *Introduction*, elevated AnxA6 levels reduce cholesterol, caveolin-1, and the number of caveolae at the cell surface (Cubells *et al.*, 2007, 2008). On the other hand, it is well documented that reduced cholesterol levels in Golgi membranes interfere with post-Golgi vesicle transport (Wang *et al.*, 2000; Pol *et al.*, 2005). Furthermore, as SNARE proteins are concentrated in cholesterol-dependent clusters that define docking and fusion sites for exocytosis (Lang *et al.*, 2001) and participate in post-Golgi transport (Choudhury *et al.*, 2006), we hypothesized that Golgi cholesterol depletion induced by high amounts of AnxA6 might interfere with the cellular functioning of SNAP23 and syntaxin-4, two t-SNARE proteins involved in the secretory pathway.

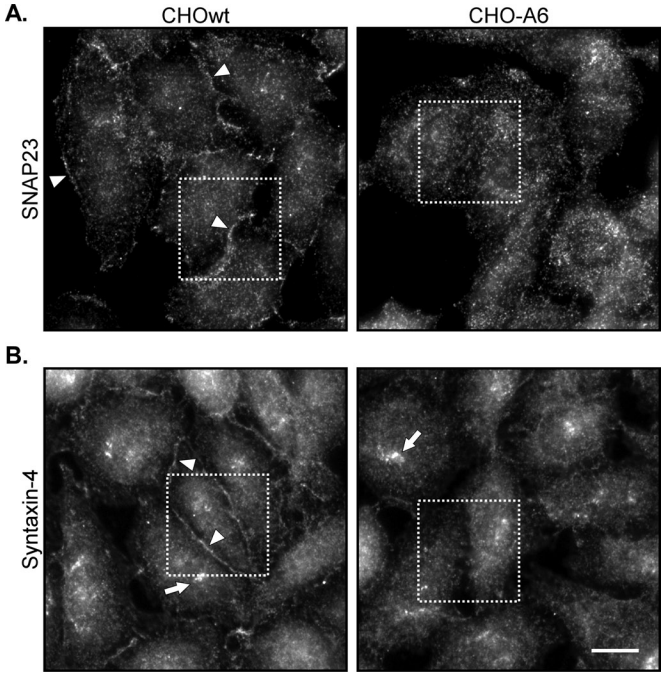

FIGURE 1: Localization of SNAP23 and syntaxin-4 in AnxA6-overexpressing cells. CHOwt and CHO-A6 cells were grown on coverslips, fixed in methanol, and immunolabeled with (A) anti-SNAP23 and (B) anti–syntaxin-4. Endogenous SNAP23 and syntaxin-4 are located at the PM of CHOwt (arrowheads) and predominantly in intracellular punctate structures of CHO-A6 cells (arrows). Squares indicate areas of interest for comparison. Scale bar: 10 μm.

Ectopic expression of AnxA6 alters SNAP23 and syntaxin-4 localization in CHO cells

We first examined whether increased levels of AnxA6 affect t-SNAREs (SNAP23 and syntaxin-4) that have been linked to cholesterol-rich membrane domains at the PM. Therefore we initially compared the localization of SNAP23 and syntaxin-4 in CHO wild-type (CHOwt) and the well-characterized CHO-A6 cell line (Grewal *et al.*, 2000, 2005; Pons *et al.*, 2001; Rentero *et al.*, 2006; Cubells *et al.*, 2007, 2008). CHOwt cells express low amounts of AnxA6, whereas AnxA6 levels in CHO-A6 cells are similar to AnxA6 expression levels observed in other commonly used cell lines, such as HeLa and NRK (Cubells *et al.*, 2007).

CHOwt and CHO-A6 cells were fixed in cold methanol and immunostained with antibodies to SNAP23 and syntaxin-4. In CHOwt cells, endogenous SNAP23 and syntaxin-4 staining was mainly observed at the PM (Figure 1, A and B, arrowheads), but also in small punctate structures throughout the cytoplasm. However, in CHO-A6, PM association of SNAP23 and syntaxin-4 was strongly reduced, particularly the prominent labeling in the contact area between adjacent cells, which showed a rather homogeneous punctate pattern throughout the cell. Anti–syntaxin-4 also labeled perinuclear structures (Figure 1B, arrows). Quantification of these studies (see below) revealed a significant reduction of SNAP23 and syntaxin-4 membrane labeling in CHO-A6 cells (see *Materials and Methods* for details). These observations were independent of cell confluency (unpublished data) and not due to changes in SNAP23 and syntaxin-4 expression levels upon AnxA6 overexpression, as CHOwt and CHO-A6 (the predominant model used in the present study) express comparable amounts of SNAP23, syntaxin-4, and other SNARE proteins (e.g., NSF and VAMP3) that might impact on SNAP23/syntaxin-4 localization (see Figures 3, A–B, and 4, A–B). Importantly, analysis of localization of other SNARE proteins, such as syntaxin-3, VAMP2, VAMP3, and VAMP8, showed similar cellular distributions in CHOwt and CHO-A6 cells (Supplemental Figure S1).

Hence AnxA6-induced changes in SNARE localization appeared specific for several cholesterol-sensitive t-SNAREs. As AnxA2 has been found to interact with caveolin–cholesterol complexes (Smart *et al.*, 2004) and translocates to membrane rafts, possibly to regulate/stabilize raft formation (Oliferenko *et al.*, 1999), we analyzed the distribution of SNAP23 and syntaxin-4 in CHOwt cells overexpressing AnxA2-green fluorescent protein (GFP). In AnxA2-GFP–transfected cells, no changes in the distribution of these t-SNAREs was observed, further emphasizing that AnxA6-induced alterations in SNAP23, and syntaxin-4 localization are likely specific within the annexin family (Figure S2).

Importantly, similar results were obtained when anti-SNAP23 or anti–syntaxin-4 staining was compared in A431 wild-type (A431wt) cells, which lack endogenous AnxA6 (Smythe *et al.*, 1994; Grewal *et al.*, 2005), and the stable AnxA6-expressing A431-A6 cell line (Figure S3, A and B). In contrast, stable AnxA6 knockdown HeLa cells (HeLa-A6-KD) showed increased SNAP23 and syntaxin-4 PM localization (Figure S3C). Thus AnxA6-induced t-SNARE mislocalizations are not specific for the CHO-A6 cell line and elevation of AnxA6 levels per se correlates with reduced amounts of these t-SNAREs at the PM.

Three separate microscopy approaches to improve the analysis and to quantify the alterations in the distribution of SNAP23 and syntaxin-4 in CHO-A6 cells were performed: total internal reflection fluorescence microscopy (TIRF-M), isolated membrane sheets, and super-resolution stimulated emission depletion (STED) microscopy. Figure 2, A and C, shows representative images of the immunocytochemical analysis of SNAP23 and syntaxin-4 performed by TIRF-M (see *Materials and Methods* for details). CHOwt and CHO-A6 cells were fixed and labeled with antibodies to SNAP23 and syntaxin-4, and the basal PM was examined. At the same TIRF excitation depth (80–150 nm), discrete SNARE clusters in both cell lines were observed. Further supporting mislocalization of t-SNAREs in cells with elevated AnxA6 levels, the mean fluorescence intensity of each cluster and the number (density) and area coverage of SNAP23 and syntaxin-4 clusters decreased significantly in CHO-A6 cells (Figure 2, B and D, respectively). Similarly, while the quantitative analysis of isolated membrane sheets from CHOwt and CHO-A6 cells stained with anti-SNAP23 or anti–syntaxin-4 showed an overall distribution of clusters similar to other cell lines (Lang *et al.*, 2001), area coverage and density of SNAP23 and syntaxin-4 clusters was reduced in CHO-A6 cells (Figure S4).

To further characterize these SNARE clusters, we imaged CHOwt and CHO-A6 cells using superresolution STED microscopy. STED microscopy achieves nanoscale resolution, which gives a higher lateral resolution than TIRF or confocal microscopy. As shown by TIRF-M, the number and the intensity of SNAP23 and syntaxin-4 membrane clusters decreased in CHO-A6 cells. Interestingly, STED microscopy revealed that the individual area of clusters was almost identical in CHOwt and CHO-A6 cells (145 ± 35 nm, syntaxin-4; 136 ± 30 nm, SNAP23). These findings correspond to similar electron microscopy data obtained from endothelial cells (Predescu *et al.*, 2005; Figure 2, E–H). Together, results from TIRF and STED microscopy strongly suggest that CHO-A6 cells not only have fewer cholesterol-dependent SNARE clusters in the PM but also that these clusters appear to contain a lower density of molecules per cluster.

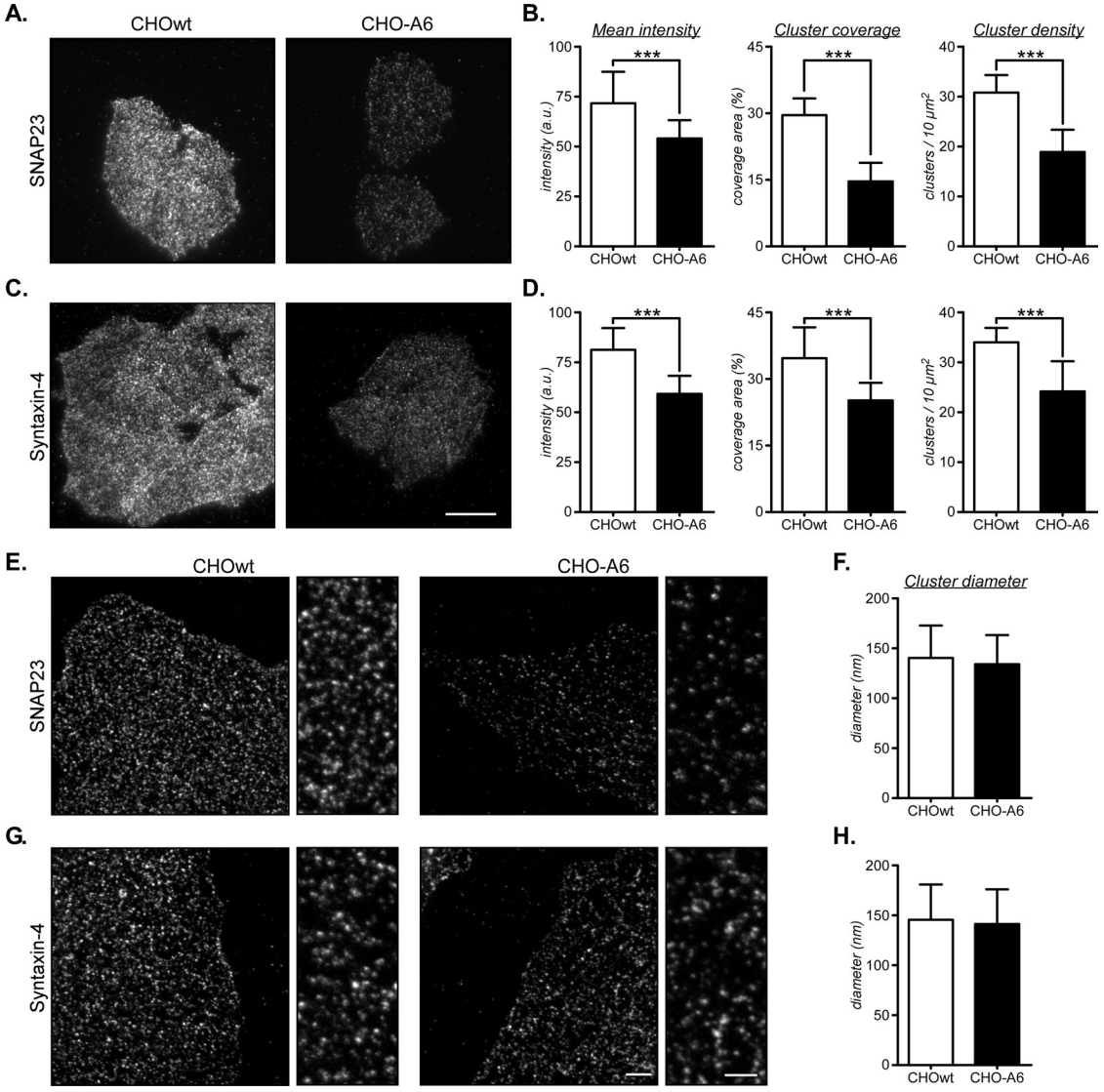

FIGURE 2: TIRF-M and STED microscopy show altered SNAP23 and syntaxin-4 membrane clusters in CHO-A6 cells. CHOwt and CHO-A6 cells were grown on coverslips, fixed, permeabilized, and immunolabeled with (A) anti-SNAP23 and (C) anti–syntaxin-4. Distribution and quantification of SNAP23 and syntaxin-4 clusters at the basal PM was analyzed by TIRF-M as indicated (B and D; see *Materials and Methods* for details). The mean intensity, cluster coverage, and cluster density ± SD of (B) SNAP23 and (D) syntaxin-4 clusters in CHOwt and CHO-A6 reflects the data obtained for the sum of clusters visible in the evanescent field of a minimum of 20 cells. At least 10,000 clusters per cell line were analyzed. *** $p < 0.001$ for Student's *t* test. Scale bar: 10 µm. Diameters of SNARE clusters were analyzed by nano-resolution STED microscopy (E–H). Representative fields (scale bar: 2 µm) and enlarged areas (scale bar: 1 µm) show details of these clusters in CHOwt and CHO-A6. Graphical representation of cluster diameter ± SD of at least 5000 clusters of (F) SNAP23 and (H) syntaxin-4 are shown.

Characterization of SNAP23 and syntaxin-4–containing compartments in AnxA6-expressing cells

To identify whether alterations of t-SNARE protein localization in CHO-A6 cells could be confirmed by biochemical means, we first performed a crude membrane separation that, in support of the immunocytochemical data (Figures 1 and 2), indicated decreased amounts of SNAP23 and syntaxin-4 in PM fractions of CHO-A6 cells (unpublished data). As these t-SNAREs could be accumulating in the Golgi apparatus (see below), we next isolated crude Golgi membranes and compared the relative amounts and distribution of SNAP23 and syntaxin-4 with Rab4 (early endosomes), Na^+/K^+-ATPase (PM), Sec61 (endoplasmic reticulum), and mannosidase II (ManII), a *cis*-Golgi marker. CHOwt and CHO-A6 express substantial amounts of both SNAP23 and syntaxin-4, as judged by similar and strong signal intensity using specific antibodies (see whole-cell lysate [WCL] in Figure 3A). Increased amounts of SNAP23 and syntaxin-4 were clearly detectable in Golgi fractions isolated from CHO-A6 cells (Figure 3A).

The integrity of t-SNARE localization at the PM is characterized by t-SNARE association with a distinct class of cholesterol-rich microdomains (membrane rafts) or detergent-resistant membranes (DRMs; Puri and Roche, 2006). To determine whether reduced cell surface localization of t-SNAREs in CHO-A6 cells would correlate with changes in their association with DRMs, we next compared the distribution of SNAP23 and syntaxin-4 from CHOwt and CHO-A6 cells in DRMs and soluble membrane fractions (Salaun *et al.*, 2005).

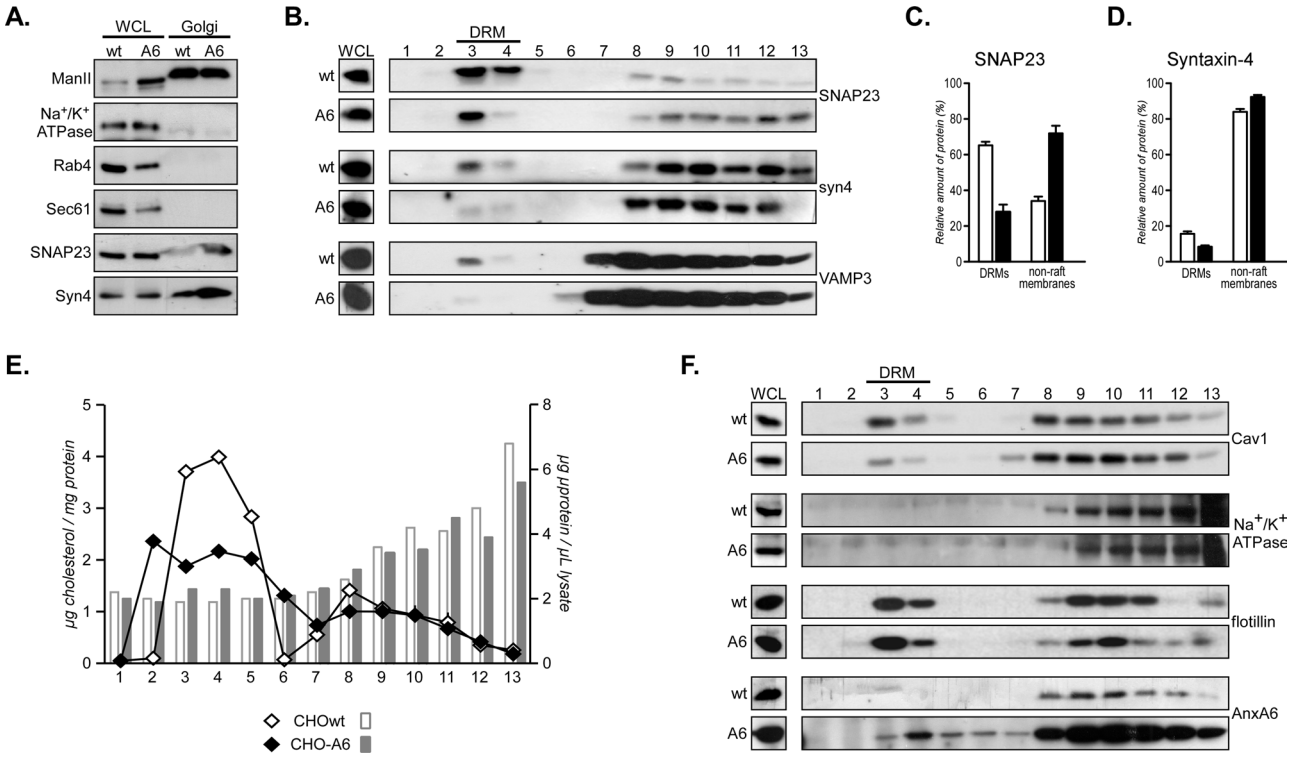

FIGURE 3: Reduced association of SNARE proteins with DRMs in AnxA6-expressing CHO cells. (A) Crude Golgi membranes from CHOwt and CHO-A6 cells were isolated as described (see *Materials and Methods*). The enrichment of Golgi fractions was assessed by Western blot analysis and comparison with whole-cell lysates (WCL) using anti–mannosidase II (ManII) *cis*-Golgi marker, anti–Na^+K^+-ATPase (PM), anti-Rab4 (early endosomes), and anti-Sec61 (endoplasmic reticulum). Increased amounts of SNAP23 and syntaxin-4 were detected in Golgi fractions from CHO-A6 cells. (B and F) Analysis of raft-associated SNARE proteins in CHOwt and CHO-A6. Crude membranes of both cell lines were solubilized in cold 1% Triton X-100 and separated on discontinuous sucrose gradients (see *Materials and Methods* for details). Fractions were collected from top to bottom and analyzed by Western blotting for the distribution of (B) SNAP23, synataxin-4, and VAMP3, and (F) caveolin-1 (Cav1), Na^+K^+-ATPase, flotillin, and AnxA6 as control. Fractions corresponding to DRMs (membrane rafts; fractions 3 and 4) are indicated. Nonmembrane raft–associated proteins are found in the soluble fractions 7–13. Representative gradients are shown. The relative amount ± SD of (C) SNAP23 and (D) syntaxin-4 in DRMs from three independent experiments was quantified and is given in (%). White bars, CHOwt; black bars, CHO-A6 cells. (E) Cholesterol (µg/mg cell protein) and protein content of each fraction was determined (see *Materials and Methods*).

Crude membranes from CHOwt and CHO-A6 cells were solubilized in cold 1% Triton X-100, and DRMs were isolated on the basis of flotation after ultracentrifugation in a discontinuous sucrose gradient (45%/35%/5%). Consistent with other reports, the majority of SNAP23 (65.3 ± 2.9%) in CHOwt cells was found in DRM fractions (Figure 3B, fractions 3 and 4), with smaller amounts of SNAP23 distributing in the soluble fractions (Figure 3B, fractions 7–13). Only a small, but significant, amount of syntaxin-4 (15.7 ± 2.0%) was detected in DRMs of CHOwt cells. In contrast, SNAP23 and syntaxin-4 from fractionated CHO-A6 cell lysates showed a strongly reduced association with DRMs (42 and 50%, respectively) and were predominantly found in the soluble (non-DRM) fractions (Figure 3B; for quantification see Figure 3, C–D). We also observed reduced amounts of VAMP3 in DRM fractions of CHO-A6 cells (Figure 3B). In contrast to SNAP23 and syntaxin-4 (Figures 1–5), these findings were not associated with altered VAMP3 localization (Figure S1C) but could be linked to changes in t-SNARE assembly in CHO-A6 cells (see Figure 4). Consistent with reduced amounts of caveolin-1 and caveolae at the cell surface of CHO-A6 (Cubells *et al.*, 2007), these cells also exhibited reduced amounts of caveolin-1 in the DRM fractions (Figure 3F). Interestingly, not only the distribution of non–raft-associated proteins (Na^+/K^+-ATPase), but also flotillin, another protein marker for raft membranes and DRMs, is comparable in both cell lines (Figure 3F).

To examine whether reduced amounts of t-SNAREs and caveolin-1 in DRM fractions of CHO-A6 would correlate with reduced cholesterol levels, we determined the cholesterol content in each fraction using an enzymatic-based assay (Figure 3E). As expected, DRM fractions containing SNAP23, syntaxin-4, caveolin, and flotillin from CHOwt cell lysates were highly enriched with cholesterol (Figure 3E, fractions 3–5). In contrast, DRMs isolated from CHO-A6 cells contained ~40–50% less cholesterol. These findings are consistent with our previous data, showing a similar magnitude of cholesterol reduction in purified PM fractions (Cubells *et al.*, 2007). Altogether, this suggests that loss of cholesterol in DRMs at the cell surface of CHO-A6 cells contributes to the reduced cell surface localization and DRM association of t-SNAREs SNAP23 and syntaxin-4.

AnxA6 interferes with SNAP23/syntaxin-4 assembly

To determine whether AnxA6-induced changes in the cellular distribution and DRM association of SNAP23 and syntaxin-4 could be indicative of altered t-SNARE complex composition, we performed

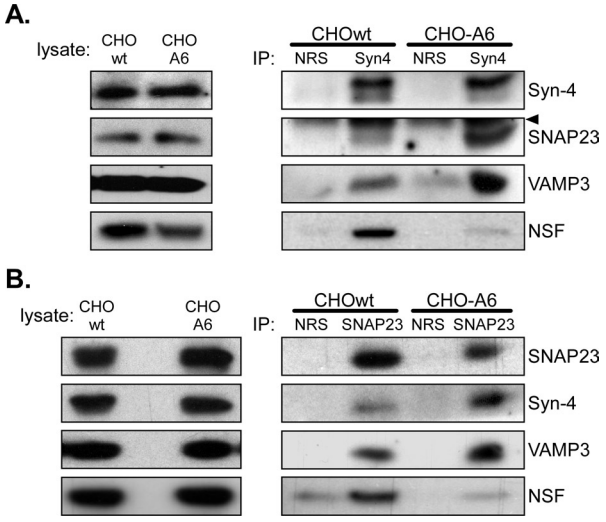

FIGURE 4: Increased SNAP23/syntaxin-4 assembly in CHO-A6 cells. Cell lysates from CHOwt and CHO-A6 cells were immunprecipitated (IP) with control (NRS), (A) anti–syntaxin-4, or (B) anti-SNAP23 and analyzed by Western blotting for coimmunoprecipitation of SNAP23, syntaxin-4, VAMP3, and NSF, as indicated. Blots from representative experiments are shown. NRS, normal rabbit serum. The amount of total syntaxin-4, SNAP23, VAMP3, and NSF in cell lysates used for immunoprecipitations from both cell lines is comparable and shown. A small arrowhead in (A) indicates nonspecific immunoglobulin G staining.

immunoprecipitation experiments. Similar amounts of syntaxin-4 could be immunoprecipitated from CHOwt and CHO-A6 cells (Figure 4A). Most strikingly, while only small amounts of SNAP23 coprecipitated with syntaxin-4 in CHOwt, large amounts of SNAP23 were identified in syntaxin-4 immunocomplexes from CHO-A6 cells (Figure 4A). Reciprocal coimmunoprecipitations confirmed enhanced SNAP23/syntaxin-4 assembly in CHO-A6 compared with CHOwt cells (Figure 4B).

SNAP23 and syntaxin-4 interacting with VAMP3 (cellubrevin) in endothelial cells has been described (Matsushita *et al.*, 2003; Pulido *et al.*, 2010). Therefore we also examined the capacity of VAMP3 to form ternary complexes with SNAP23 and syntaxin-4 in CHOwt and CHO-A6 cells. Similar to the weak interaction of SNAP23 with syntaxin-4 in CHOwt, only small amounts of VAMP3 coimmunoprecipitated with SNAP23 and syntaxin-4 in the control cells. In contrast, the amount of VAMP3 in SNAP23 and syntaxin-4 forming t-SNARE complexes was highly increased in CHO-A6 cells (Figure 4, A and B). Interestingly, increased VAMP3 assembly with SNAP23 and syntaxin-4 in CHO-A6 cells appeared specific, as the amount of VAMP3 in syntaxin-6 immunocomplexes (Wendler and Tooze, 2001) was comparable in CHOwt and CHO-A6 cells (unpublished data). Since the ATPase *N*-ethylmaleimide-sensitive factor (NSF) mediates the disassembly of SNARE complexes, we next examined if NSF was present in the t-SNARE complexes of CHO-A6 cells containing SNAP23 and syntaxin-4. Further indicating perturbed t-SNARE complex formation and the inability of SNAP23/syntaxin-4 complexes to properly disassemble (possibly in the Golgi; see below), syntaxin-4 and SNAP23 immunocomplexes of AnxA6-expressing cells contained only residual amounts of NSF (Figure 4, A and B; Sudhof and Rothman, 2009). As mentioned above, the expression levels of SNAP23, syntaxin-4, and NSF were comparable in both CHOwt and CHO-A6, further emphasizing that ectopic expression of AnxA6 impacts on cellular distribution, but not protein expression, of these t-SNAREs (Figure 4, A–B; see also Figure 3, A–B).

SNAP23 and syntaxin-4 have been implicated in caveolin transport and/or caveolae functioning (Predescu *et al.*, 2005; Choudhury *et al.*, 2006). As CHO-A6 cells are characterized by 1) reduced cholesterol levels in DRMs (Figure 3C) and the PM (Cubells *et al.*, 2007), 2) cholesterol-dependent caveolin retention, and 3) increased amounts of SNAP23/syntaxin-4 in crude Golgi membranes (Figure 3A), we reasoned that SNAP23 and syntaxin-4 could be accumulating in the Golgi of CHO-A6 cells.

CHOwt and CHO-A6 cells were therefore transiently transfected with caveolin-GFP, fixed, immunolabeled with anti-GM130 and anti-SNAP23 or anti–syntaxin-4, and analyzed by confocal microscopy (Figure 5, A and B). In CHO-A6 cells, some scattered, punctate SNAP23/syntaxin-4–stained structures that did not colocalize with early (EEA1, Rab4, Rab5), late (Rab7, LBPA), or recycling (Rab11) markers (unpublished data) were observed, possibly corresponding to non-*cis*-derived Golgi vesicles or secretory vesicles. More importantly, these experiments revealed, in support of increased SNAP23/syntaxin-4 assembly in Golgi membranes of CHO-A6, that endogenous SNAP23 and syntaxin-4, GM130, and ectopically expressed caveolin-GFP partially colocalized in the *cis*-Golgi region. This colocalization was not observed in CHOwt cells.

In summary, reduced SNAP23 and syntaxin-4 cell surface localization and association with DRMs is associated with a retention/sequestration of SNAP23/syntaxin-4/VAMP3 complexes in the Golgi apparatus.

Late endosomal cholesterol and cPLA$_2$ regulate t-SNARE localization

Treatment of cells expressing low/undetectable AnxA6 levels (CHOwt, A431wt) with 3-β-[2-(diethylamino) ethoxy] androst-5-en-17-one (U18666A), a hydrophobic polyamine that promotes accumulation of cholesterol in late endosomes, or methyl arachidonyl fluorophosphonate (MAFP), a Ca^{2+}-dependent cPLA$_2$ inhibitor, abrogated caveolin export from the Golgi (Cubells *et al.*, 2007, 2008). These studies established that late endosomal cholesterol drives cholesterol-dependent cPLA$_2$ recruitment and activity in the Golgi to promote caveolin export. Utilizing these pharmacological agents, we examined whether inhibition of late endosomal cholesterol export or cPLA$_2$ activity could be responsible for reduced cell surface localization of SNAP23 and syntaxin-4 in CHO-A6 cells.

First, CHOwt cells were incubated with U18666A, fixed, and immunolabeled with anti-SNAP23 and anti–syntaxin-4 (Figure 6). Quantification of membrane labeling showed a differential effect of U18666A on the membrane location for these t-SNAREs (representative images are shown in Figure S5). Consistent with U18666A inducing an AnxA6-like phenotype, as judged by reduced Golgi and PM cholesterol levels, PM staining of SNAP23 and syntaxin-4 was reduced by 23 and 48%, respectively, compared with nontreated CHOwt cells (Figure 6, A and B; for quantification see *Materials and Methods*). Similar to previous studies on caveolin-1, U18666A did not significantly alter the localization of either t-SNARE in CHO-A6 cells compared with nontreated CHO-A6 cells (Cubells *et al.*, 2007). In CHOwt cells, inhibition of cholesterol export from late endosomes reduces SNAP23 and syntaxin-4 cell surface association, mimicking the effect of AnxA6 overexpression on the localization of these two t-SNAREs.

Inhibition of cholesterol export from late endosomes reduces cholesterol delivery back to the PM (Neufeld *et al.*, 1996; Wojtanik and Liscum, 2003; Cubells *et al.*, 2007). This could contribute to reduced cell surface association of SNAP23 and syntaxin-4 in CHO-A6

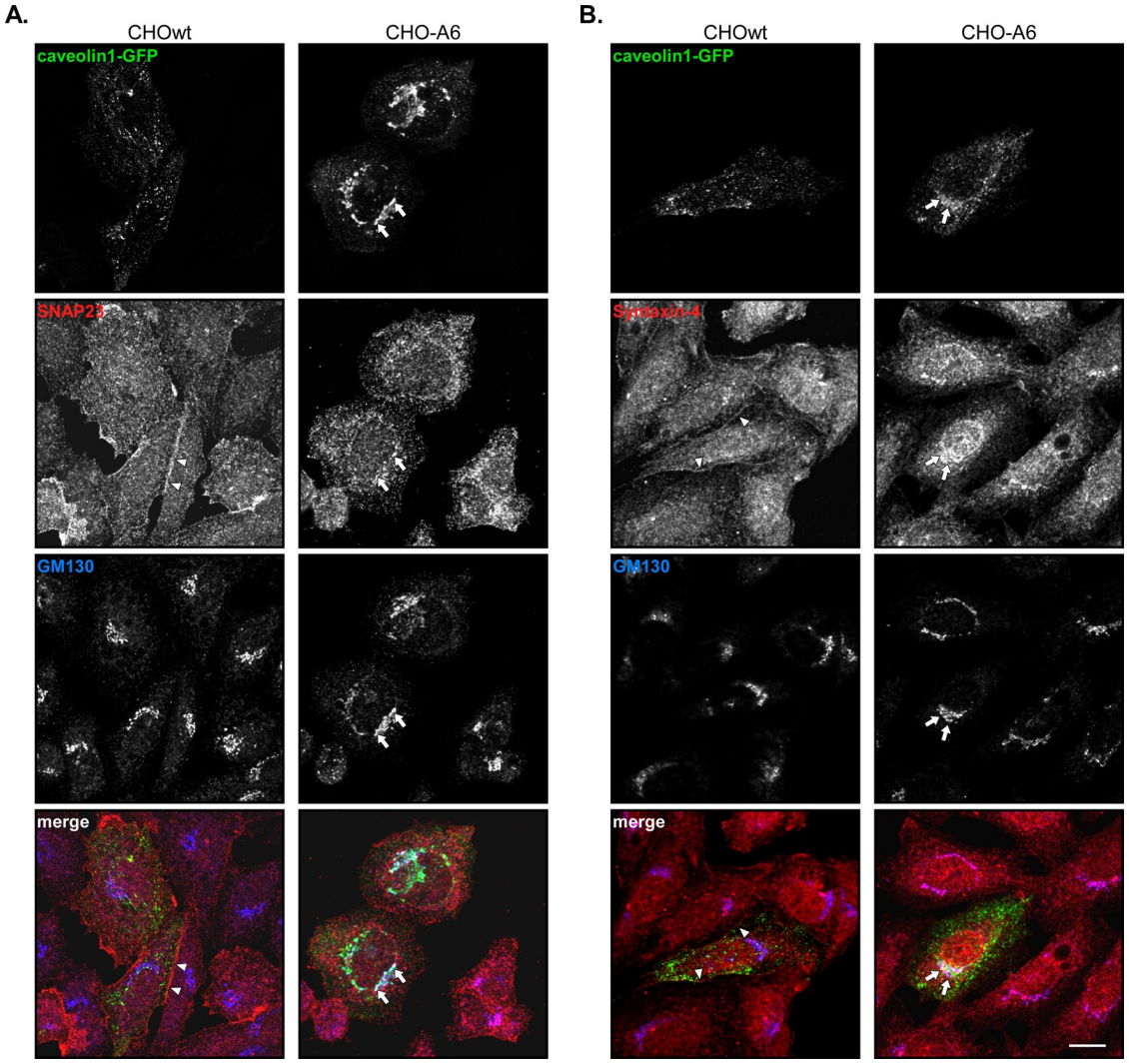

FIGURE 5: SNAP23 and syntaxin-4 colocalize with caveolin-1 in Golgi membranes of AnxA6-expressing CHO cells. CHOwt and CHO-A6 cells grown on coverslips were transfected with caveolin-EGFP (cav-GFP; green), fixed in methanol, and immunolabeled with (A) anti-SNAP23 or (B) anti–syntaxin-4 (red) and anti-GM130 (blue), as indicated, and analyzed by confocal microcopy. Arrowheads highlight syntaxin-4 or SNAP23 at the PM and small arrows point to the colocalization in the perinuclear Golgi region of CHO-A6 cells. Scale bar: 10 μm.

cells. Therefore CHOwt (and CHO-A6 cells, unpublished data) were treated with methyl-β-cyclodextrin (CD) to remove cholesterol from the PM, fixed, and stained for SNAP23 and syntaxin-4. While PM association of SNAP23 and syntaxin-4 was still apparent after 30 min in the presence of CD (Figure 6C, arrows), extended incubation with CD (60–90 min) completely removed both of these t-SNAREs from the PM. Intense intracellular (Figure 6C, arrowheads), Golgi-like labeling in the perinuclear region of CD-incubated CHOwt cells, especially with anti–syntaxin-4, was similar to that observed in CHO-A6 cells (Figure 1B). Taken together, these findings strongly indicate that AnxA6 modulates cholesterol pools in late endosomes and at the cell surface to alter t-SNARE localization and functioning at the PM and Golgi.

We previously proposed late endosomal cholesterol as a driver for cholesterol-dependent recruitment of $cPLA_2$ to the Golgi, followed by $cPLA_2$-dependent vesiculation events that promote caveolin export to the cell surface (Cubells *et al.*, 2008). Therefore we next examined the effect of $cPLA_2$ inhibition on t-SNARE localization. Indeed, MAFP strongly reduced PM labeling of SNAP23 (36%) and syntaxin-4 (60%) in CHOwt cells (Figure 6, A–B). As expected, MAFP cells had much smaller impact on SNAP23 and syntaxin-4 membrane association in CHO-A6 cells. Thus and similar to our previous reports for caveolin-1 transport, retention of cholesterol in late endosomes (U18666A), as well as $cPLA_2$ inhibition (MAFP), crucially affects SNAP23 and syntaxin-4 distribution within the PM in CHOwt cells, indicating that similar mechanisms are in place in cells with elevated AnxA6 levels. The slightly differential behavior of syntaxin-4 and SNAP23 toward U18666A and MAFP indicates that additional or independent mechanisms might be involved in determining their localization/assembly.

NPC1 and exogenous cholesterol restore t-SNARE distribution in CHO-A6 cells

The majority of AnxA6 proteins are targeted to the PM upon cell activation. In addition, a pool of AnxA6 proteins is recruited to late endosomes in a cholesterol-dependent manner, even in the absence of Ca^{2+} (de Diego *et al.*, 2002). This pool of AnxA6 proteins appears to interact with NPC1 and interferes with cholesterol export

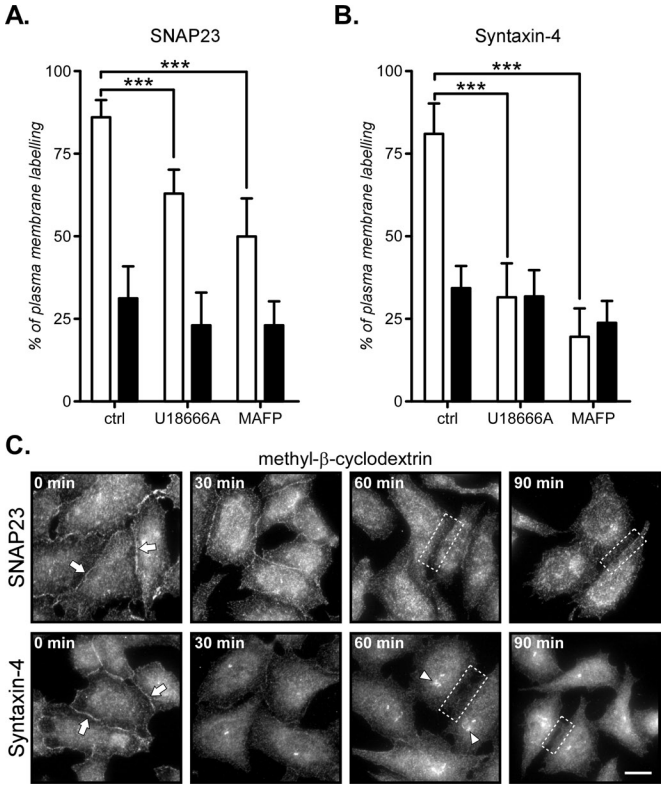

FIGURE 6: Sequestration of cholesterol in late endosomes and $cPLA_2$ inhibition alters the cellular distribution of t-SNARE proteins in CHO cells. CHOwt and CHO-A6 cells were grown on coverslips, incubated with or without U18666A or MAFP, fixed, permeabilized, and immunolabeled with anti-SNAP23 or anti–syntaxin-4, as indicated. Quantification of PM labeling (%) ± SD for (A) SNAP23 or (B) syntaxin-4 in control (ctrl)-, U18666A-, and MAFP-incubated CHOwt (white bars) and CHO-A6 cells (black bars) is given. Approximately 300 cells per cell line per treatment were analyzed. *** $p < 0.001$ for Student's *t* test. (C) CHOwt cells were treated with CD for 0, 30, 60, and 90 min, fixed, and stained with anti-SNAP23 and anti–syntaxin-4, as indicated. Arrows point at SNAP23 and syntaxin-4 at the PM (t = 0 min). Rectangles indicate areas at the PM without SNAP23 and syntaxin-4 labeling (t = 60–90 min). Arrowheads highlight SNAP23 and syntaxin-4 localization in perinuclear structures (t = 60–90 min). Scale bar: 10 μm.

from the late endosomal compartment (Cubells *et al.*, 2007). However, given the proposed function for several annexins, including AnxA6, as regulators of membrane microdomain formation via direct protein–protein and protein–lipid interaction at the cell surface, we aimed to rule out that AnxA6 at the PM could be responsible for the mislocalization of t-SNAREs.

We therefore analyzed SNAP23 and syntaxin-4 localization in CHO cells expressing AnxA6 fused to the membrane anchors of H- and K-Ras (AnxA6-GFP-tH, AnxA6-GFP-tK; Monastyrskaya *et al.*, 2009b). CHOwt cells transiently transfected with AnxA6-GFP-tK and -tH were immunolabeled with anti-SNAP23 or anti–syntaxin-4 antibodies and analyzed by confocal microscopy (Figure 7, A and B). In cells expressing membrane-anchored AnxA6, cholesterol distribution, as judged by filipin staining, and caveolin immunostaining, was comparable to controls, indicating no major changes in membrane microdomains at the cell surface upon overexpression of lipid-anchored AnxA6 (unpublished data). Most strikingly, independent of H- or K-Ras anchors, membrane targeting of AnxA6 did not alter the distribution of SNAP23 or syntaxin-4 at the PM, where they colocalized with AnxA6 (Figure 7, A and B, arrowheads). Furthermore, CHOwt cells expressing membrane-anchored AnxA6 did not show perturbed cholesterol (filipin) or caveolin-1 staining patterns characteristic for CHO-A6 cells (unpublished data). These findings strongly suggest that constitutive PM association of AnxA6 does not affect cell surface association of SNAP23 or syntaxin-4.

As further proof of principle and similar to the stable CHO-A6 cell line, transiently expressed AnxA6-YFP in CHOwt cells induced a significant loss of SNAP23 and syntaxin-4 membrane staining compared with nontransfected controls (Figure 7, C and D). In all of these control experiments, levels of transiently expressed AnxA6 ± membrane anchors were comparable to those observed in the CHO-A6 cell line (unpublished data). In summary, these results strongly indicate that reduced membrane labeling of SNAP23 and syntaxin-4 is not due to the physical association of AnxA6 with the PM, but through AnxA6 pools regulating cholesterol transport pathways in other compartments, such as late endosomes.

We have previously shown that AnxA6 coimmunoprecipitates with NPC1, a cholesterol transporter in the late endosomal/lysosomal compartment. We also demonstrated that ectopic expression of NPC1 restored the cellular distribution of cholesterol and caveolin-1 in CHO-A6 cells (Cubells *et al.*, 2007). Given the findings described above, we speculated that NPC1 overexpression in CHO-A6 cells could reestablish SNAP23 and syntaxin-4 cell surface labeling. As hypothesized, expression of NPC1 in CHO-A6 cells reinstated the PM location of both SNAP23 and syntaxin-4 (Figure 8). It is tempting to conclude from these experiments that reduced cholesterol export from late endosomes in CHO-A6 cells is responsible for t-SNARE rearrangements. The release of these t-SNAREs (SNAP23, syntaxin-4) toward post-Golgi pathways—as shown for caveolin-1—can be rescued by overexpression of NPC1.

Finally, we reasoned that not only NPC1 overexpression, but also exogenous cholesterol would restore the exit from the Golgi complex of t-SNARE proteins in CHO-A6 on route to the cell surface, which presumably requires cholesterol. Indeed, addition of cholesterol (90 min) completely reestablished the membrane association and pattern of SNAP23 (Figure 9A) and syntaxin-4 (Figure 9B) in CHO-A6 cells. Thus, as shown for caveolin (Cubells *et al.*, 2007), addition of exogenous cholesterol in CHO-A6 cells appears to overcome the inhibitory action of AnxA6 on late endosomal cholesterol export, allowing release of SNAP23 and syntaxin-4 from the Golgi membranes, and thereby restoring their PM location.

Annexin A6 overexpression reduces fibronectin and TNF-α secretion

Since SNAP23 and syntaxin-4 regulate post-Golgi exocytic pathways (Hong, 2005), we hypothesized that elevated AnxA6 levels causing SNAP23/syntaxin-4 mislocalization should be associated with loss of SNAP23/syntaxin-4 function, as judged by reduced secretion of cargo (along the exocytic pathway). Therefore we measured the amount of fibronectin (FN) secreted into the media of CHOwt and CHO-A6 cells (Aggeler *et al.*, 1982; Figure 10A). Consistent with AnxA6 inhibiting t-SNARE function, FN secretion was strongly reduced in CHO-A6 cells after 24 h (31%) and 48 h (53%). Similarly, stable expression of AnxA6 in A431 cells (A431-A6; Figure 10C) or AnxA6 overexpression and knockdown in HuH7 (HuH7-A6 and HuH7-A6-KD) hepatoma cells correlated with decreased and increased FN secretion, respectively (Figure 10B).

Finally, we determined the secretion of tumor necrosis factor α (TNF-α) upon lipopolysaccharide (LPS) stimulation, which has been shown to require SNAP23 and syntaxin-4 (Kay *et al.*, 2006; Manderson *et al.*, 2007), using an enzyme-linked immunosorbent

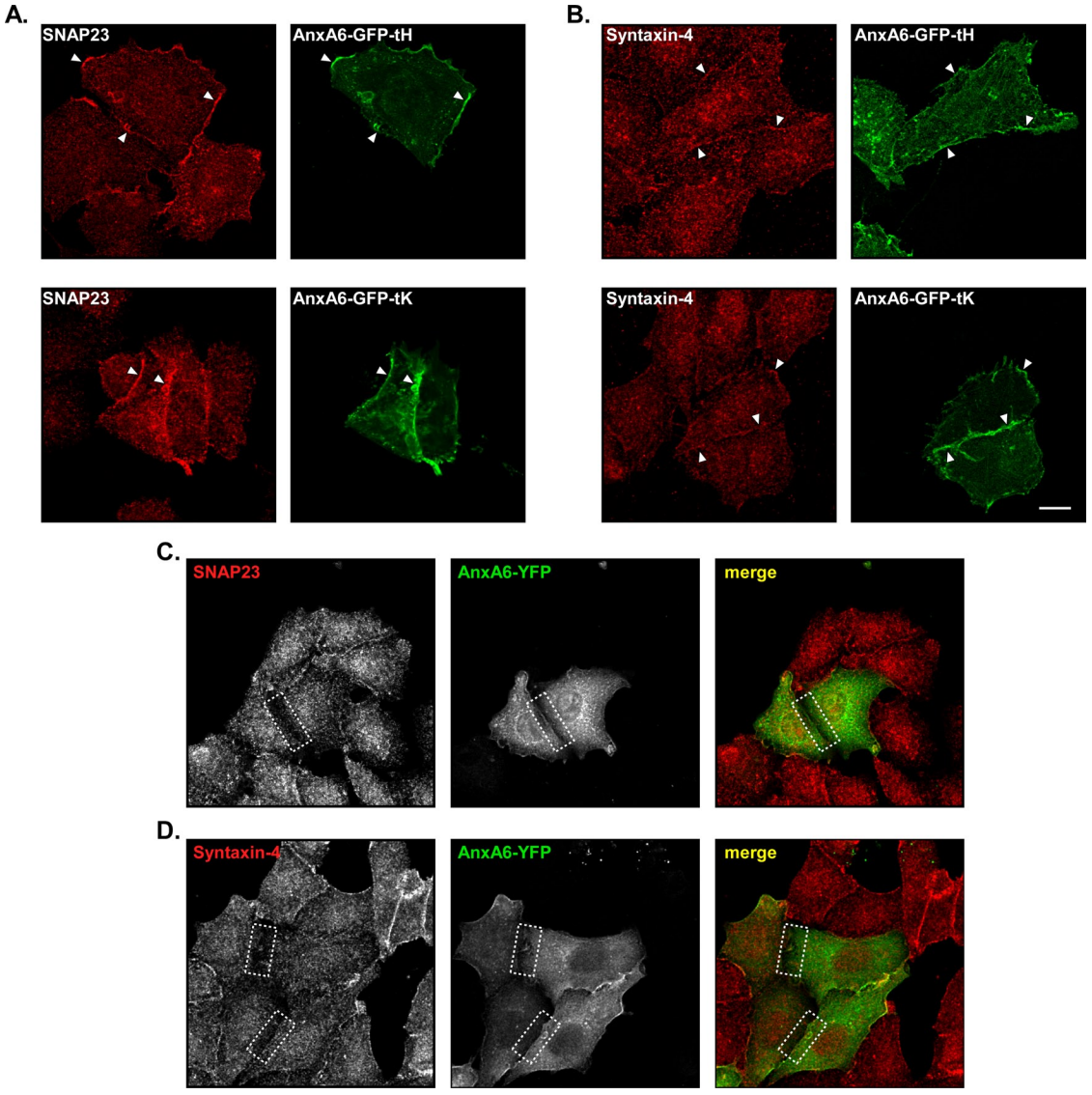

FIGURE 7: Membrane-anchored AnxA6 does not alter the localization of SNAP23 and syntaxin-4. CHOwt cells were grown on coverslips, transfected with membrane-anchored AnxA6-GFP-tH and -tK (green), fixed, permeabilized, and immunolabeled with (A) anti-SNAP23 or (B) anti–syntaxin-4 (red), as indicated. Arrowheads point at SNAP23 and syntaxin-4 colocalizing with AnxA6. CHOwt cells were grown on coverslips, transfected with AnxA6-YFP (green), and then labeled with (C) anti-SNAP23 and (D) anti–syntaxin-4 (red). Rectangles indicate loss of SNAP23 and syntaxin-4 cell surface labeling in cell–cell contact regions of AnxA6-YFP–expressing cells. Scale bar: 10 μm.

assay (ELISA)-based assay in A431 cells ± AnxA6 and in MDA-MB-436 and MDA-MB-468, two breast cancer cell lines characterized by high and low levels of AnxA6, respectively (Vila de Muga *et al.*, 2009). In support of high AnxA6 levels inhibiting SNAP23/syntaxin-4–dependent exocytic pathways, secretion of TNF-α in A431wt cells was significantly higher compared with A431-A6 cells (Figure 10D). Furthermore, MDA-MB-436 with high AnxA6 levels showed much less LPS-inducible TNF-α secretion compared with MDA-MB-468 cells (Figure 10D). It should be noted that Okayama and coworkers determined exocytosis of secreted alkaline phosphatase (SEAP) to remain unchanged upon RNA interference knockdown of SNAP23 and syntaxin-4 (Okayama *et al.*, 2007). Incomplete gene silencing; compensation through other SNAREs; different combinations of SNAREs being required for SEAP and FN/cytokine release, possibly along multiple and different intracellular routes; and AnxA6-induced changes that go beyond alterations in cholesterol homeostasis could explain these differences. Altogether, our findings support a model of AnxA6 levels determining the involvement of SNAP23 and syntaxin-4 in constitutive FN/cytokine release through changes in Golgi cholesterol.

DISCUSSION

This study shows that impaired cholesterol egress from late endosomes in cells with high AnxA6 levels is associated with the altered cellular distribution and assembly of SNAP23, and syntaxin-4, both t-SNARE proteins of the secretory pathway. Ectopic expression of Niemann-Pick type C1 (NPC1) or exogenous cholesterol restores the location of SNAP23 and syntaxin-4 within the PM. Conversely, U18666A-induced accumulation of late endosomal cholesterol and MAFP-mediated $cPLA_2$ inhibition induce an AnxA6-like phenotype in control CHOwt cells with low AnxA6 levels. Therefore we conclude that reduced cholesterol availability in AnxA6-overexpressing

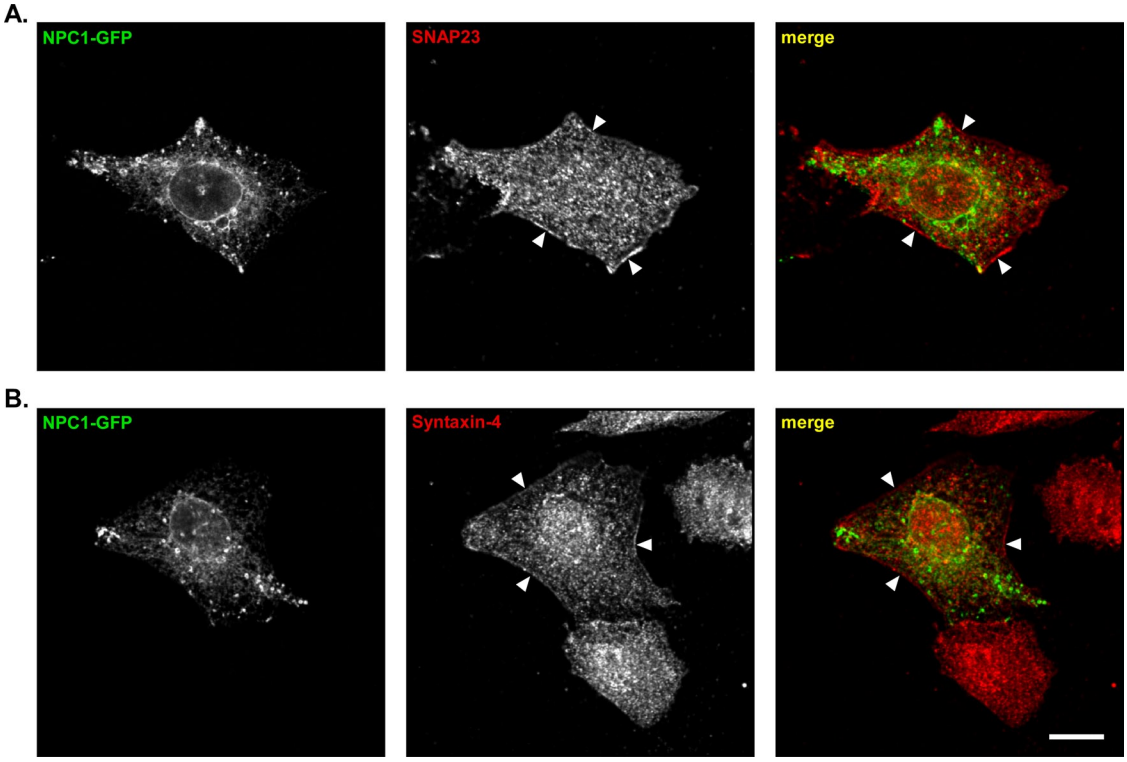

FIGURE 8: Expression of NPC1 restores the membrane localization of t-SNAREs in CHO-A6 cells. CHO-A6 cells were transfected with NPC1-GFP (green), fixed, and immunolabeled with (A) anti-SNAP23 or (B) anti–syntaxin-4 (red), as indicated. Arrowheads point at SNAP23 and syntaxin-4 labeling at the PM. Scale bar: 10 μm.

cells perturbs $cPLA_2$ translocation to the Golgi, a process necessary for driving cholesterol-dependent t-SNARE complex localization, assembly, and functioning. Importantly, t-SNARE accumulation in Golgi membranes of cells with high AnxA6 levels correlates with reduced secretion of cargo along the constitutive and SNAP23/syntaxin-4–dependent secretory pathway.

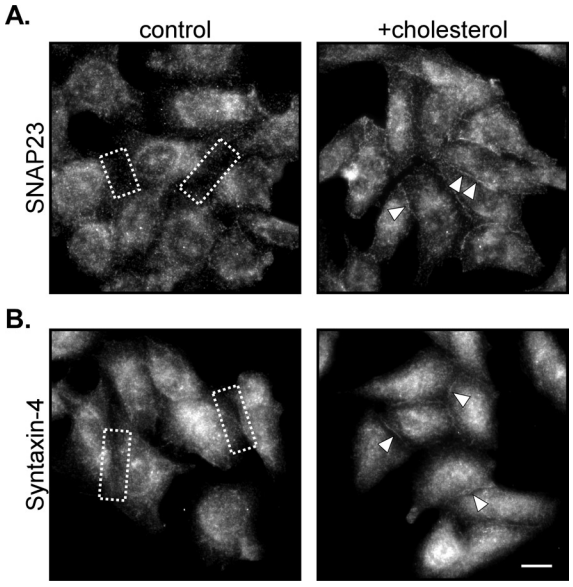

FIGURE 9: Exogenous cholesterol restores SNAP23 and syntaxin-4 PM localization. CHO-A6 cells were grown on coverslips, incubated with (+ cholesterol) or without (control) exogenous cholesterol for 90 min, fixed, and immunolabeled with (A) anti-SNAP23 or (B) anti–syntaxin-4. Rectangles highlight PM regions without SNAP23 and syntaxin-4 staining. Arrowheads point to the PM of cholesterol-treated CHO-A6 cells. Scale bar: 10 μm.

AnxA6-mediated SNARE regulation

Annexins have long been considered as potential regulators of cholesterol-rich membrane microdomains at the PM (Gerke *et al.*, 2005; Lemmon, 2008; Grewal *et al.*, 2010; Enrich *et al.*, 2011). This was considered to occur mainly via annexins interacting directly with other regulatory proteins or lipids, thereby creating and stabilizing membrane microenvironments. Accordingly, annexins possibly alter the lipidic environment—including cholesterol—at the PM (Ayala-Sanmartin, 2001; Domon *et al.*, 2010). In addition, annexins could potentially interact with key players regulating membrane dynamics at the cell surface, such as members of the SNARE superfamily, including t-SNAREs, within membrane rafts (Puri and Roche, 2006). However, to our knowledge, only AnxA2 has been identified as binding SNAP23 in alveolar type II cells (Wang *et al.*, 2007) and interacting with VAMP2 for exocytosis in chromaffin cells (Umbrecht-Jenck *et al.*, 2010).

Along these lines, AnxA6 is predominantly found at the PM, and although AnxA6 has not yet been identified in t-SNARE complexes, one could speculate that these AnxA6 pools may participate in the regulation of SNARE membrane association and assembly. For instance, AnxA6 could compete with SNARE proteins in PM microdomains through interacting and/or rearranging the cortical actin cytoskeleton (Monastyrskaya *et al.*, 2009b), potentially impairing the formation of syntaxin-4–actin protein complexes (Band *et al.*, 2002). As has been proposed for other annexins in this framework of molecular rearrangements, elevated AnxA6 levels at the PM could potentially alter phospholipid asymmetry, which could then modify the affinity/efficiency of SNAREs to bind and form clusters. However, SNAP23 and syntaxin-4 localization remained unchanged in cells

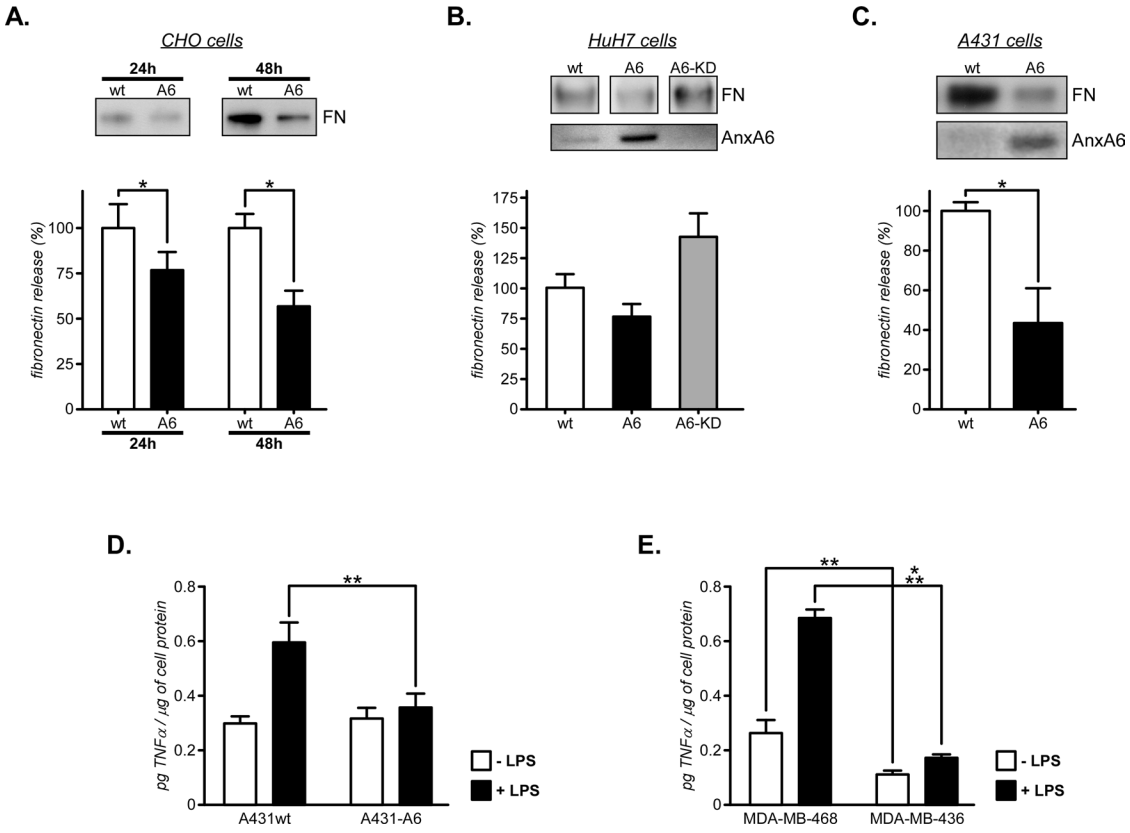

FIGURE 10: Fibronectin and TNF-α secretion in AnxA6-overexpressing cells. (A) CHOwt and CHO-A6; (B) HuH7wt, HuH7-A6, and HuH7-A6-KD; and (C) A431wt and A431-A6 cells were cultured to confluence and then serum-starved for 24 h. The media was collected and analyzed by Western blotting for the amount of secreted fibronectin (FN). (D) A431wt and A431-A6 and (E) MDA-MB-436 and MDA-MB-468 cells were stimulated with 100 ng/ml LPS for 16 h. Aliquots of the media were analyzed for the amount of secreted TNF-α by using a commercial ELISA.

expressing membrane-anchored AnxA6. While we cannot completely rule out a role of PM–bound AnxA6 in microdomain formation, altered properties of membrane-anchored AnxA6 in control experiments (Figure 7), and t-SNARE functioning in other cell types, we conclude from our studies in CHO, A431, and HeLa that AnxA6 protein pools acting in other cellular compartments are responsible for SNAP23 and syntaxin-4 mislocalization in certain cell types. Results presented here strongly suggest that AnxA6 indirectly regulates SNAP23 and syntaxin-4 localization/assembly via reducing the availability of cholesterol at the Golgi and PM. The formation/stability of t-SNARE–containing membrane clusters (e.g., syntaxin-3, syntaxin-4, SNAP23) at the cell surface seems to possess differential sensitivity toward cholesterol, depending on the cell type analyzed. Certainly, treatment with CD in MDCK, endothelial, or CHO cells reveals similar trends, but slightly different impacts on SNARE cluster formation (Predescu *et al.*, 2005; Low *et al.*, 2006). Importantly, the formation of SNARE clusters at the PM depends on the transport of specific SNARE proteins through the secretory pathway and the concomitant availability of cholesterol, which regulates post-Golgi trafficking in a complex and stepwise manner. As CHO-A6 cells are characterized by an increased coimmunoprecipitation of SNAP23 and syntaxin-4, which correlates with significant colocalization of both proteins with caveolin-1 in the Golgi, one can speculate that insufficient cholesterol delivery to the Golgi is the driving force that causes retention of SNAP23 and syntaxin-4, which ultimately explains the differential spatiotemporal formation of SNARE complexes in CHO-A6 cells.

Consistent with AnxA6 inhibiting caveolin-1 export through inhibition of cholesterol-dependent $cPLA_2$ recruitment and vesiculation events in the Golgi (Cubells *et al.*, 2008), $cPLA_2$ inhibition in CHOwt strongly reduced PM labeling of SNAP23 and syntaxin-4. As outlined below, these observations correlate with several studies that implicated $cPLA_2$ and its product, arachidonic acid (AA), in SNARE trafficking and complex formation. Polyunsaturated fatty acids (PUFAs), including AA, are also modulators of syntaxins. PUFAs promote membrane curvature and, indirectly, the fission/fusion of vesicles. In this manner, $cPLA_2$ primes membrane fusion through AA production to induce the release of secretory vesicles (Latham and Meunier, 2007). It has been proposed that local $cPLA_2$ action results in transiently high AA concentrations at the membrane where syntaxins reside, before AA diffuses deeper into the cytosol. Furthermore, syntaxins appear to sense high PUFA concentrations, which would stimulate SNARE interactions. AA induces the so-called "syntaxin-opened" conformation, which forms a Munc18-containing t-SNARE complex. Depletion of AA inhibits syntaxin-4 from forming SNARE complexes (Connell *et al.*, 2007). And last, addition of AA or treatment with $cPLA_2$ is sufficient to stimulate SNARE complex formation in vitro (Rickman and Davletov, 2005).

Inhibition of late endosomal cholesterol export alters the location and function of t-SNARE proteins in AnxA6-overexpressing cells

Microscopic studies and biochemical analysis of DRMs demonstrated that cholesterol depletion disturbs SNARE microdomains

(Chamberlain *et al.*, 2001), indicating that SNARE proteins are enriched in membrane rafts and that the integrity of SNARE-containing domains depends on cholesterol (Salaun *et al.*, 2004; Sieber *et al.*, 2006). However, uneven alterations in the distribution of SNARE proteins after cholesterol depletion have been reported, ranging from moderate to complete disintegration of SNARE domains (Lang *et al.*, 2001), indicating that lipids are important for SNARE domain integrity but that other regulatory mechanism, including additional protein–protein interactions, might also be required.

Studies presented here implicate AnxA6 expression levels as one of those yet unknown fine-tuning modulators of cholesterol-dependent SNARE microdomain and complex formation. Although increased t-SNARE endocytosis in AnxA6-overexpressing cells cannot be completely ruled out as contributing to the phenotype observed, the ability of AnxA6 to impact on SNARE localization and functioning is probably linked to its association with late endosomes, which plays a crucial role in cholesterol trafficking and homeostasis. Late endosomes are a sorting station and are capable of exporting cholesterol via vesicular (Maxfield and Tabas, 2005; Urano *et al.*, 2008) and nonvesicular (protein-mediated) transport mechanisms involving NPC1 (Garver and Heidenreich, 2002) and cytoplasmic sterol-binding proteins (e.g., oxysterol-binding protein/OSBP-related proteins [OSBP/ORPs], ORP5; Ngo *et al.*, 2010; Du *et al.*, 2011) or through StAR-related lipid transfer domain (START)-domain proteins (Soccio and Breslow, 2003; Alpy and Tomasetto, 2005; Ikonen, 2008). In CHO-A6 cells, cholesterol accumulates in late endosomes, probably due to AnxA6 interference with NPC1 activity. In these cells, AnxA6 is not only recruited to late endosomes, but also colocalizes and coimmunoprecipitates with NPC1 (Cubells *et al.*, 2007; Sztolsztener *et al.*, 2010). Moreover, in CHO-A6 cells NPC1 overexpression not only rescues cholesterol homeostasis and caveolin transport (Cubells *et al.*, 2007), but also the association of SNAP23 and syntaxin-4 with the PM. The fact that another t-SNARE, syntaxin-6, has also been linked to cholesterol transport from late endosomes to the TGN (Urano *et al.*, 2008) and caveolin transport (Choudhury *et al.*, 2006) indicates that inhibition of late endosomal cholesterol transport to the Golgi and reduced $cPLA_2$ activity via upregulated AnxA6 levels, NPC deficiency, or pharmacological $cPLA_2$ inhibitors might go beyond SNAP23 and syntaxin-4 with respect to t-SNARE functioning.

The role of AnxA6 in secretion has not been extensively investigated, but in line with the data presented here, the available evidence suggests that AnxA6 inhibits rather than potentiates the secretory process (Creutz, 1992; Donnelly and Moss, 1997; Podszywalow-Bartnicka *et al.*, 2010). We previously identified a significant diminution of vesicular stomatitis virus G protein transport (a well-characterized marker for constitutive transport through the secretory pathway) in CHO-A6 cells (Cubells *et al.*, 2007). In this paper, we provide evidence that high levels of AnxA6 reduce secretion of cargo (FN, TNF-α) that requires SNAP23 and syntaxin-4 function. In summary, the present data provides novel molecular insights into our understanding of constitutive protein secretion and identifies the delivery of late endosomal cholesterol to the Golgi as a new pathway linking cholesterol with t-SNARE functioning. Future studies will have to determine whether AnxA6 expression levels are a common determinant for late endosomal cholesterol regulation of t-SNARE localization, assembly, and functioning in various cellular processes and cell types.

MATERIALS AND METHODS

Reagents and antibodies

Nutrient Mixture Ham's F-12, DMEM/F12 (1/1), Roswell Park Memorial Institute (RPMI) 1640, and DMEM were from Biological Industries (Kibbutz Beit-Haemek, Israel). Filipin, CD, saponin, water-soluble cholesterol, and polyclonal anti-fibronectin were from Sigma-Aldrich (St. Louis, MO). Protein A was from Thermo Scientific (Pierce, Lafayette, CO). U18666A and MAFP were from BIOMOL Research Laboratories (Plymouth Meeting, PA). Paraformaldehyde was from Electron Microscopy Sciences (Hatfield, PA), and Mowiol from Calbiochem (San Diego, CA). Polyclonal antibodies anti-SNAP23, anti–syntaxin-3, anti-VAMP2, anti–syntaxin-4, and anti-AnxA6 were prepared in our laboratories and have been described elsewhere (Grewal *et al.*, 2000; Martin-Martin *et al.*, 2000; de Diego *et al.*, 2002; Torrejon-Escribano *et al.*, 2002; Raptis *et al.*, 2005). Polyclonal and monoclonal anti–caveolin-1, anti-flotillin, anti-GM130, and anti-Rab4 were from BD Transduction Laboratories (BD Biosciences, Franklin Lakes, NJ). Monoclonal anti-actin was from MP Biomedicals (Solon, OH); polyclonal anti-Sec61 and monoclonal anti-Na^+/K^+-ATPase were from Upstate (Millipore, Billerica, MA). Polyclonal anti-Rab7 was from Santa Cruz Biotechnology (Santa Cruz, CA). Anti-VAMP3 (Cellubrevin) and anti-VAMP8 (Endobrevin) were from Synaptic Systems (Göttingen, Germany). Anti-NSF was from Santa Cruz. Alexa Fluor–conjugated secondary antibodies were from Molecular Probes (Invitrogen, Carlsbad, CA). Anti–mannosidase II was kindly donated by Angel Velasco (University of Seville, Seville, Spain). Horseradish peroxidase–conjugated secondary antibodies were from Bio-Rad (Hercules, CA). The enhanced green fluorescent protein (EGFP)- and yellow fluorescent protein (YFP)-tagged caveolin-1 and AnxA6 expression vectors ± H- and K-Ras lipid anchors have been described elsewhere (Cubells *et al.*, 2007; Monastyrskaya *et al.*, 2009b; Vila de Muga *et al.*, 2009). The NPC1-GFP was kindly provided by P. G. Pentchev (National Institutes of Health [NIH], Bethesda, MD).

Cell culture

CHOwt and CHO-A6 cells were grown in Ham's F-12; A431wt, A431-A6, HeLa, HeLa-A6-KD, and HuH7 were grown in DMEM; MDA-MB-436, and MDA-MB-468 were grown in RPMI 1640 with insulin (0.3 U/ml), together with 10% fetal calf serum, L-glutamine (2 mM), penicillin (100 U/ml), and streptomycin (100 µg/ml) at 37°C, 5% CO_2. The generation of the stable AnxA6-overexpressing CHO cell line (CHO-A6) and A431 cell line (A431-A6) has been described in detail (Grewal *et al.*, 2000, 2005; Pons *et al.*, 2001; Cubells *et al.*, 2007; Vila de Muga *et al.*, 2009). To generate AnxA6-overexpressing HuH7, we transfected HuH7 cells with pcDNAanx6 (Grewal *et al.*, 2000) and selected in the presence of 1 mg/ml G418. After 2 wk, G418-resistant and AnxA6-overexpressing HuH7 cells were identified. For the generation of HeLa and HuH7 cells with stable AnxA6 knockdown (HeLa-A6-KD, HuH7-A6-KD), (1–2) × 10^6 HeLa cells were transfected with 1.5 µg SureSilencing shRNA plasmid (SABiosciences, Frederick, MD) targeting human AnxA6 at position 352–372 (5′-gcaaggacctcattgctgatt-3′) and Lipofectamine 2000 according to the manufacturer's instructions. After 48 h, cells were selected in the presence of 100 µg/ml puromycin. After 2 wk, puromyin-resistant and AnxA6-depleted colonies were identified. For transient transfections, (1–2) × 10^5 CHO cells were transfected using Effectene (Qiagen, Valencia, CA) or Lipofectamine 2000 (Invitrogen) per the manufacturer's instructions.

Cholesterol, U18666A, MAFP, and CD treatments

For the addition of cholesterol, cells were incubated with 30 µg/ml cholesterol for 90 min (premixed for 60 min in DMEM by gentle agitation). For the accumulation of cholesterol in late endosomes, cells were treated 16 h with 2 µg/ml U18666A, as described previously (de Diego *et al.*, 2002; Cubells *et al.*, 2007). Filipin staining was used

to visualize the accumulation of free cholesterol. For the inhibition of Ca^{2+}-dependent $cPLA_2$ activity, cells were incubated with 15 μM MAFP for 60 min as described previously (Grimmer *et al.*, 2005). In some experiments, cells were treated ± 10 mM CD for 0–90 min.

Immunoprecipitation

CHOwt and CHO-A6 cells were grown on 10-cm dishes, washed with phosphate-buffered saline, and solubilized in TGH buffer (1% Triton X-100, 10% glycerol, 50 mM NaCl, 50 mM HEPES, pH 7.3, 1 mM Na_3VO_4, 10 mM NaF, 1 mM phenylmethylsulfonyl fluoride [PMSF], 10 mg/ml leupeptin, 10 mg/ml aprotinin) followed by centrifugation at 12,000 × *g* for 10 min at 4°C. Protein from supernatants (500–800 μg) was incubated for 2 h with rabbit polyclonal anti–syntaxin-4 or rabbit preimmune serum as negative control, which was followed by another 60 min upon addition of protein A-Sepharose. Immunoprecipitates were washed twice in TGH supplemented with 150 mM NaCl, and then once without NaCl. For SNAP23 immunoprecipitations, the same protocol (in 50 mM Tris, 100 mM NaCl, 0.1 mM $CaCl_2$, 0.5% Triton X-100) was used (Choudhury *et al.*, 2006).

Immunofluorescence

Cells were grown on coverslips and fixed with 4% paraformaldehyde for 30 min, washed, permeabilized with 0.1% saponin for 10 min, blocked with 0.2% bovine serum albumin for 10 min, and incubated with primary and secondary antibodies as described previously (Pons *et al.*, 2000). For the syntaxin-4 and SNAP23 labeling, cells were fixed with cold methanol for 2 min. Finally, samples were mounted in Mowiol, and cells were observed using a Leica DMI 6000B epifluorescence inverted microscope equipped with an HCX PLAN APO 63×, oil-immersion objective. Images were also captured with a Leica TCS SP5 laser-scanning confocal microscope equipped with a DMI6000 inverted microscope, blue diode (405 nm), argon (458/476/488/496/514), diode-pumped solid-state (561 nm) and helium-neon (594/633 nm) lasers (Leica). To visualize the basal PM, an Olympus IX81 inverted microscope with TIRF illumination and a 1.45 numerical aperture, 150×, oil-immersion TIRF objective equipped with a diode-pumped solid-state laser operating at 488 nm was utilized (Olympus Corporation). Images were captured using a Hamamatsu Orca-ER digital camera and Olympus CellR software.

STED microscopy

Samples from CHOwt and CHO-A6 cells were fixed, stained, and mounted in Prolong as described above and imaged using a true confocal scanning (TCS) STED (Leica Microsystems) superresolution fluorescence microscope equipped with a 1.4 NA, 100× objective. Confocal images of immunostained cells were obtained for Oregon Green (syntaxin-4 and SNAP23), which was followed by imaging Oregon Green by applying STED resolution. Pixel size was 25.8 nm. STED excitation was performed with a 488-nm diode laser, depletion was achieved via a MaiTai tunable laser (Spectra-Physics, Santa Clara, CA) at 592 nm, and emission was collected at 496–578 nm using photomultiplier tubes.

Image analysis

Image analysis was performed with ImageJ software (Rasband, 1997–2011). To quantify the membrane fluorescence intensity of syntaxin-4 and SNAP23 staining in CHOwt and CHO-A6 cells, images captured using identical microscope settings were systematically screened, and the PM intensity was determined by looking for the intercellular apposed membranes. Double-blind membrane-targeting quantifications were performed for over 300 cells in independent experiments for each cell line and condition. One-way analysis of variance was applied to highlight statistical differences between the treatments.

For cluster quantification, nonedged cellular areas from TIRF and STED microscopy images were locally thresholded and clusters were selected through the ImageJ particle analysis function. For each cluster, the full width at half-maximum was determined by calculating maximum and minimum intensity locally. Cluster intensity, area, and density from raw images were then calculated. Quantitative data are expressed as the mean ± SD. A paired Student's *t* test was used to establish the statistical significance of differences between the means.

PM sheets preparation

For membrane sheet preparation (Avery *et al.*, 2000), cells were cultured on round glass coverslips coated with 0.1 mg/ml poly-L-lysine (Sigma-Aldrich), washed with KOAc buffer (25 mM HEPES, 115 mM KOAc, 25 mM $MgCl_2$, pH 7.4), sonicated with a Branson ultrasonics sonifier (model 250, 40% duty cycle, output 6; Danbury, CT), and washed with KOAc buffer. Membrane sheets were fixed for 30 min at room temperature in 4% paraformaldehyde, washed, and immunostained with primary antibody, followed by secondary A488-coupled antibody. Cell rupture was monitored by phase-contrast microscopy. Membrane sheets were always counterstained with filipin and visualized by reflection. Only intact, flat membrane sheets stained with filipin and visualized by reflection were used for quantification.

Isolation of subcellular fractions and DRMs

For the isolation of DRMs, cells were washed three times and then resuspended in 1 ml HES buffer (20 mM HEPES, 1 mM EDTA, 250 mM sucrose, pH 7.4) supplemented with 1 mM Na_3VO_4, 10 mM NaF, 1 mM PMSF, 10 μg/ml leupeptin, and 10 μg/ml aprotinin. Cells were homogenized by 10 passages through a 22-gauge needle and centrifuged at 245,000 × *g* for 90 min at 4°C. Membranes (pellet) were resuspended in 1 ml of MBS buffer (25 mM MES, 150 mM NaCl, pH 6.5) containing 1% Triton X-100 plus the protease inhibitors and were then incubated at 4°C for 20 min. Solubilized membranes were resuspended with 10 passages through a 22-gauge needle and 1 ml homogenate was added to an equal volume of 90% (wt/vol) sucrose in MBS (45% final sucrose [wt/vol]) and overlaid with 2 ml 35% sucrose and 1 ml 5% sucrose. Samples were centrifuged at 240,000 × *g* for 17 h, and 450-μl fractions from top to bottom were collected (Salaun *et al.*, 2005).

Golgi membranes were isolated from CHOwt and CHO-A6 cells as described previously (Cubells *et al.*, 2008). In some experiments, crude cellular fractionation was performed to isolate PM/low-density membrane (PM/LDM) membrane fractions using a previously described method (Martin *et al.*, 1998). All procedures were carried out at 4°C. In brief, five 10-cm plates for each condition were rinsed twice in cold phosphate-buffered saline and homogenized in HES buffer containing protease inhibitors (10 μg/ml aprotinin, 10 μg/ml leupeptin, and 250 μM PMSF) by 20 passes through a 23-gauge needle. The homogenate was centrifuged at 16,000 × *g* for 15 min. The pellet was washed, layered onto 1.12 M sucrose, and centrifuged at 100,000 × *g* for 70 min at 4°C. The membranous layer above the sucrose cushion contained highly enriched PMs. Supernatant from the initial spin was subsequently centrifuged at 38,700 × *g* for 20 min. The resulting supernatant contained the LDM-enriched fraction.

Western blot analysis

CHOwt and CHO-A6 cell lysates, gradients, and immunoprecipitations were separated by SDS–PAGE and transferred to Immobilon-P (Millipore) and then incubated with primary antibodies and the appropriate peroxidase-conjugated secondary antibodies and enhanced chemiluminescence detection (Amersham Biosciences, GE Healthcare, Waukesha, WI). Protein content was measured by the methods of Lowry and Bradford, respectively (Lowry *et al.*, 1951; Bradford, 1976).

Cholesterol measurements

The amount of cholesterol in DRMs and soluble membrane fractions was determined using the Amplex Red Cholesterol Assay Kit (Molecular Probes) as previously described (Cubells *et al.*, 2007). Results were normalized to total cellular protein.

Fibronectin and TNF-α secretion

CHO (3×10^6 cells) in Ham's F-12 containing 10% FCS and HuH7 (3×10^5 cells) and A431 (1.5×10^5 cells) in DMEM containing 5% FCS were grown for 48 h (to confluence). Cells were washed and incubated in serum-free media for an additional 24 h (48 h for CHO cells). Media were collected and analyzed by Western blotting for the amount of secreted fibronectin. Positive immunoreactive bands were quantified densitometrically using ImageJ and normalized for the number of cells.

For the measurement of TNF-α secretion, 5×10^5 A431, MDA-MB-436, and MDA-MB-468 cells (in triplicate) were stimulated with 100 ng/ml LPS (Sigma-Aldrich) for 16 h. TNF-α secretion in the media was determined by ELISA (BD Biosciences PharMingen; Kay *et al.*, 2006) according to the instructions of the manufacturer and normalized to total cellular protein.

ACKNOWLEDGMENTS

This research was supported by grants BFU2009-10335, CONSOLIDER-INGENIO CSD2009-00016 from Ministerio de Innovación, Ciencia y Tecnología and PI040236 from Fundació Marató TV3 (Barcelona, Spain) to C.E. T.G. is supported by the National Health and Medical Research Council of Australia (NHMRC; 510293, 510294) and the University of Sydney (2010-02681). C.R. thanks the Beatriu de Pinós fellowship (Generalitat de Catalunya). M.R. and A.A. are supported by fellowships from Ministerio de Innovación, Ciencia y Tecnología. P.W. is a recipient of a cofunded National Heart Foundation/NHMRC postgraduate scholarship. We thank Laia Cubells for her participation in the initiation of this project, Maria Calvo (Centres Científics i Tecnològics, Universitat de Barcelona/IDIBAPS); TIRF-M images were obtained at the Institute for Research in Biomedicine (IRB, Barcelona) with the technical assistance of Anna Lladó and Julien Colombelli and STED images in the CRG-Centre for Genomic Regulation (Barcelona) thanks to Timo Zimmermann.

REFERENCES

Aggeler J, Kapp LN, Tseng SC, Werb Z (1982). Regulation of protein secretion in Chinese hamster ovary cells by cell cycle position and cell density. Plasminogen activator, procollagen fibronectin. Exp Cell Res 139, 275–283.

Alpy F, Tomasetto C (2005). Give lipids a START: the StAR-related lipid transfer (START) domain in mammals. J Cell Sci 118, 2791–2801.

Avery J, Ellis DJ, Lang T, Holroyd P, Riedel D, Henderson RM, Edwardson JM, Jahn R (2000). A cell-free system for regulated exocytosis in PC12 cells. J Cell Biol 148, 317–324.

Ayala-Sanmartin J (2001). Cholesterol enhances phospholipid binding and aggregation of annexins by their core domain. Biochem Biophys Res Commun 283, 72–79.

Babiychuk EB, Monastyrskaya K, Draeger A (2008). Fluorescent annexin A1 reveals dynamics of ceramide platforms in living cells. Traffic 9, 1757–1775.

Band AM, Ali H, Vartiainen MK, Welti S, Lappalainen P, Olkkonen VM, Kuismanen E (2002). Endogenous plasma membrane t-SNARE syntaxin 4 is present in rab11 positive endosomal membranes and associates with cortical actin cytoskeleton. FEBS Lett 531, 513–519.

Bradford MM (1976). A rapid and sensitive method for the quantitation of microgram quantities of protein utilizing the principle of protein-dye binding. Anal Biochem 72, 248–254.

Bryant NJ, Govers R, James DE (2002). Regulated transport of the glucose transporter GLUT4. Nat Rev Mol Cell Biol 3, 267–277.

Chamberlain LH, Burgoyne RD, Gould GW (2001). SNARE proteins are highly enriched in lipid rafts in PC12 cells: implications for the spatial control of exocytosis. Proc Natl Acad Sci USA 98, 5619–5624.

Choudhury A, Marks DL, Proctor KM, Gould GW, Pagano RE (2006). Regulation of caveolar endocytosis by syntaxin 6-dependent delivery of membrane components to the cell surface. Nat Cell Biol 8, 317–328.

Connell E, Darios F, Broersen K, Gatsby N, Peak-Chew SY, Rickman C, Davletov B (2007). Mechanism of arachidonic acid action on syntaxin-Munc18. EMBO Rep 8, 414–419.

Creutz CE (1992). The annexins and exocytosis. Science 258, 924–931.

Cubells L, de Muga SV, Tebar F, Bonventre JV, Balsinde J, Pol A, Grewal T, Enrich C (2008). Annexin A6-induced inhibition of cytoplasmic phospholipase A2 is linked to caveolin-1 export from the Golgi. J Biol Chem 283, 10174–10183.

Cubells L *et al.* (2007). Annexin A6-induced alterations in cholesterol transport and caveolin export from the Golgi complex. Traffic 8, 1568–1589.

de Diego I, Schwartz F, Siegfried H, Dauterstedt P, Heeren J, Beisiegel U, Enrich C, Grewal T (2002). Cholesterol modulates the membrane binding and intracellular distribution of annexin 6. J Biol Chem 277, 32187–32194.

Domon MM, Matar G, Strzelecka-Kiliszek A, Bandorowicz-Pikula J, Pikula S, Besson F (2010). Interaction of annexin A6 with cholesterol rich membranes is pH-dependent and mediated by the sterol OH. J Colloid Interface Sci 346, 436–441.

Donnelly SR, Moss SE (1997). Annexins in the secretory pathway. Cell Mol Life Sci 53, 533–538.

Du X, Kumar J, Ferguson C, Schulz TA, Ong YS, Hong W, Prinz WA, Parton RG, Brown AJ, Yang H (2011). A role for oxysterol-binding protein-related protein 5 in endosomal cholesterol trafficking. J Cell Biol 192, 121–135.

Enrich C, Rentero C, de Muga SV, Reverter M, Mulay V, Wood P, Koese M, Grewal T (2011). Annexin A6-linking Ca(2+) signaling with cholesterol transport. Biochim Biophys Acta 1813, 935–947.

Fiedler K, Lafont F, Parton RG, Simons K (1995). Annexin XIIIb: a novel epithelial specific annexin is implicated in vesicular traffic to the apical plasma membrane. J Cell Biol 128, 1043–1053.

Foster LJ, De Hoog CL, Mann M (2003). Unbiased quantitative proteomics of lipid rafts reveals high specificity for signaling factors. Proc Natl Acad Sci USA 100, 5813–5818.

Garver WS, Heidenreich RA (2002). The Niemann-Pick C proteins and trafficking of cholesterol through the late endosomal/lysosomal system. Curr Mol Med 2, 485–505.

Gerke V, Creutz CE, Moss SE (2005). Annexins: linking Ca2+ signalling to membrane dynamics. Nat Rev Mol Cell Biol 6, 449–461.

Gerke V, Moss SE (2002). Annexins: from structure to function. Physiol Rev 82, 331–371.

Goebeler V, Poeter M, Zeuschner D, Gerke V, Rescher U (2008). Annexin A8 regulates late endosome organization and function. Mol Biol Cell 19, 5267–5278.

Grewal T, Enrich C (2006). Molecular mechanisms involved in Ras inactivation: the annexin A6-p120GAP complex. Bioessays 28, 1211–1220.

Grewal T, Enrich C (2009). Annexins–modulators of EGF receptor signalling and trafficking. Cell Signal 21, 847–858.

Grewal T *et al.* (2005). Annexin A6 stimulates the membrane recruitment of p120GAP to modulate Ras and Raf-1 activity. Oncogene 24, 5809–5820.

Grewal T, Heeren J, Mewawala D, Schnitgerhans T, Wendt D, Salomon G, Enrich C, Beisiegel U, Jackle S (2000). Annexin VI stimulates endocytosis and is involved in the trafficking of low density lipoprotein to the prelysosomal compartment. J Biol Chem 275, 33806–33813.

Grewal T, Koese M, Rentero C, Enrich C (2010). Annexin A6-regulator of the EGFR/Ras signalling pathway and cholesterol homeostasis. Int J Biochem Cell Biol 42, 580–584.

Grimmer S, Ying M, Walchli S, van Deurs B, Sandvig K (2005). Golgi vesiculation induced by cholesterol occurs by a dynamin- and cPLA2-dependent mechanism. Traffic 6, 144–156.
Hong W (2005). SNAREs and traffic. Biochim Biophys Acta 1744, 493–517.
Ikonen E (2008). Cellular cholesterol trafficking and compartmentalization. Nat Rev Mol Cell Biol 9, 125–138.
Jackle S, Beisiegel U, Rinninger F, Buck F, Grigoleit A, Block A, Groger I, Greten H, Windler E (1994). Annexin VI, a marker protein of hepatocytic endosomes. J Biol Chem 269, 1026–1032.
Kamal A, Ying Y, Anderson RG (1998). Annexin VI-mediated loss of spectrin during coated pit budding is coupled to delivery of LDL to lysosomes. J Cell Biol 142, 937–947.
Kay JG, Murray RZ, Pagan JK, Stow JL (2006). Cytokine secretion via cholesterol-rich lipid raft-associated SNAREs at the phagocytic cup. J Biol Chem 281, 11949–11954.
Lafont F, Verkade P, Galli T, Wimmer C, Louvard D, Simons K (1999). Raft association of SNAP receptors acting in apical trafficking in Madin-Darby canine kidney cells. Proc Natl Acad Sci USA 96, 3734–3738.
Lang T (2007). SNARE proteins and "membrane rafts." J Physiol 585, 693–698.
Lang T, Bruns D, Wenzel D, Riedel D, Holroyd P, Thiele C, Jahn R (2001). SNAREs are concentrated in cholesterol-dependent clusters that define docking and fusion sites for exocytosis. EMBO J 20, 2202–2213.
Latham CF, Meunier FA (2007). Munc18a: Munc-y business in mediating exocytosis. Int J Biochem Cell Biol 39, 1576–1581.
Lemmon MA (2008). Membrane recognition by phospholipid-binding domains. Nat Rev Mol Cell Biol 9, 99–111.
Leung SM, Chen D, DasGupta BR, Whiteheart SW, Apodaca G (1998). SNAP-23 requirement for transferrin recycling in streptolysinO-permeabilized Madin-Darby canine kidney cells. J Biol Chem 273, 17732–17741.
Low SH, Chapin SJ, Wimmer C, Whiteheart SW, Komuves LG, Mostov KE, Weimbs T (1998). The SNARE machinery is involved in apical plasma membrane trafficking in MDCK cells. J Cell Biol 141, 1503–1513.
Low SH, Vasanji A, Nanduri J, He M, Sharma N, Koo M, Drazba J, Weimbs T (2006). Syntaxins 3 and 4 are concentrated in separate clusters on the plasma membrane before the establishment of cell polarity. Mol Biol Cell 17, 977–989.
Lowry OH, Rosebrough NJ, Farr AL, Randall RJ (1951). Protein measurement with the Folin phenol reagent. J Biol Chem 193, 265–275.
Manderson AP, Kay JG, Hammond LA, Brown DL, Stow JL (2007). Subcompartments of the macrophage recycling endosome direct the differential secretion of IL-6 and TNFα J Cell Biol 178, 57–69.
Martin LB, Shewan A, Millar CA, Gould GW, James DE (1998). Vesicle-associated membrane protein 2 plays a specific role in the insulin-dependent trafficking of the facilitative glucose transporter GLUT4 in 3T3-L1 adipocytes. J Biol Chem 273, 1444–1452.
Martin-Martin B, Nabokina SM, Blasi J, Lazo PA, Mollinedo F (2000). Involvement of SNAP-23 and syntaxin 6 in human neutrophil exocytosis. Blood 96, 2574–2583.
Matsushita K *et al*. (2003). Nitric oxide regulates exocytosis by S-nitrosylation of N-ethylmaleimide-sensitive factor. Cell 115, 139–150.
Maxfield FR, Tabas I (2005). Role of cholesterol and lipid organization in disease. Nature 438, 612–621.
Mayran N, Parton RG, Gruenberg J (2003). Annexin II regulates multivesicular endosome biogenesis in the degradation pathway of animal cells. EMBO J 22, 3242–3253.
Monastyrskaya K, Babiychuk EB, Draeger A (2009a). The annexins: spatial and temporal coordination of signaling events during cellular stress. Cell Mol Life Sci 66, 2623–2642.
Monastyrskaya K, Babiychuk EB, Hostettler A, Wood P, Grewal T, Draeger A (2009b). Plasma membrane-associated annexin A6 reduces Ca^{2+} entry by stabilizing the cortical actin cytoskeleton. J Biol Chem 284, 17227–17242.
Morel E, Parton RG, Gruenberg J (2009). Annexin A2-dependent polymerization of actin mediates endosome biogenesis. Dev Cell 16, 445–457.
Neufeld EB, Cooney AM, Pitha J, Dawidowicz EA, Dwyer NK, Pentchev PG, Blanchette-Mackie EJ (1996). Intracellular trafficking of cholesterol monitored with a cyclodextrin. J Biol Chem 271, 21604–21613.
Ngo MH, Colbourne TR, Ridgway ND (2010). Functional implications of sterol transport by the oxysterol-binding protein gene family. Biochem J 429, 13–24.
Okayama M, Arakawa T, Mizoguchi I, Tajima Y, Takuma T (2007). SNAP-23 is not essential for constitutive exocytosis in HeLa cells. FEBS Lett 581, 4583–4588.
Oliferenko S, Paiha K, Harder T, Gerke V, Schwarzler C, Schwarz H, Beug H, Gunthert U, Huber LA (1999). Analysis of CD44-containing lipid rafts: recruitment of annexin II and stabilization by the actin cytoskeleton. J Cell Biol 146, 843–854.
Podszywalow-Bartnicka P, Kosiorek M, Piwocka K, Sikora E, Zablocki K, Pikula S (2010). Role of annexin A6 isoforms in catecholamine secretion by PC12 cells: distinct influence on calcium response. J Cell Biochem 111, 168–178.
Pol A, Martin S, Fernandez MA, Ingelmo-Torres M, Ferguson C, Enrich C, Parton RG (2005). Cholesterol and fatty acids regulate dynamic caveolin trafficking through the Golgi complex and between the cell surface and lipid bodies. Mol Biol Cell 16, 2091–2105.
Pol A, Ortega D, Enrich C (1997). Identification of cytoskeleton-associated proteins in isolated rat liver endosomes. Biochem J 327, 741–746.
Pons M, Grewal T, Rius E, Schnitgerhans T, Jackle S, Enrich C (2001). Evidence for the involvement of annexin 6 in the trafficking between the endocytic compartment and lysosomes. Exp Cell Res 269, 13–22.
Pons M, Ihrke G, Koch S, Biermer M, Pol A, Grewal T, Jackle S, Enrich C (2000). Late endocytic compartments are major sites of annexin VI localization in NRK fibroblasts and polarized WIF-B hepatoma cells. Exp Cell Res 257, 33–47.
Predescu SA, Predescu DN, Shimizu K, Klein IK, Malik AB (2005). Cholesterol-dependent syntaxin-4 and SNAP-23 clustering regulates caveolar fusion with the endothelial plasma membrane. J Biol Chem 280, 37130–37138.
Pulido IR, Jahn R, Gerke V (2010). VAMP3 is associated with endothelial Weibel-Palade bodies and participates in their Ca(2+)-dependent exocytosis. Biochim Biophys Acta 1813, 1038–1044.
Puri N, Roche PA (2006). Ternary SNARE complexes are enriched in lipid rafts during mast cell exocytosis. Traffic 7, 1482–1494.
Rao SK, Huynh C, Proux-Gillardeaux V, Galli T, Andrews NW (2004). Identification of SNAREs involved in synaptotagmin VII-regulated lysosomal exocytosis. J Biol Chem 279, 20471–20479.
Raptis A, Torrejon-Escribano B, Gomez de Aranda I, Blasi J (2005). Distribution of synaptobrevin/VAMP 1 and 2 in rat brain. J Chem Neuroanat 30, 201–211.
Rasband WS (1997–2011). ImageJ. National Institutes of Health, Bethesda, MD. http://imagej.nih.gov/ij (accessed 9 September 2011).
Rentero C, *et al*. (2006). Inhibition of H-Ras and MAPK is compensated by PKC-dependent pathways in annexin A6 expressing cells. Cell Signal 18, 1006–1016.
Rickman C, Davletov B (2005). Arachidonic acid allows SNARE complex formation in the presence of Munc18. Chem Biol 12, 545–553.
Salaun C, Gould GW, Chamberlain LH (2005). Lipid raft association of SNARE proteins regulates exocytosis in PC12 cells. J Biol Chem 280, 19449–19453.
Salaun C, James DJ, Chamberlain LH (2004). Lipid rafts and the regulation of exocytosis. Traffic 5, 255–264.
Schnitzer JE, Liu J, Oh P (1995). Endothelial caveolae have the molecular transport machinery for vesicle budding, docking, and fusion including VAMP, NSF, SNAP, annexins, and GTPases. J Biol Chem 270, 14399–14404.
Sieber JJ, Willig KI, Heintzmann R, Hell SW, Lang T (2006). The SNARE motif is essential for the formation of syntaxin clusters in the plasma membrane. Biophys J 90, 2843–2851.
Smart EJ, De Rose RA, Farber SA (2004). Annexin 2-caveolin 1 complex is a target of ezetimibe and regulates intestinal cholesterol transport. Proc Natl Acad Sci USA 101, 3450–3455.
Smythe E, Smith PD, Jacob SM, Theobald J, Moss SE (1994). Endocytosis occurs independently of annexin VI in human A431 cells. J Cell Biol 124, 301–306.
Soccio RE, Breslow JL (2003). StAR-related lipid transfer (START) proteins: mediators of intracellular lipid metabolism. J Biol Chem 278, 22183–22186.
St-Denis JF, Cabaniols JP, Cushman SW, Roche PA (1999). SNAP-23 participates in SNARE complex assembly in rat adipose cells. Biochem J 338, 709–715.
Sudhof TC, Rothman JE (2009). Membrane fusion: grappling with SNARE and SM proteins. Science 323, 474–477.
Sztolsztener ME, Strzelecka-Kiliszek A, Pikula S, Tylki-Szymanska A, Bandorowicz-Pikula J (2010). Cholesterol as a factor regulating intracellular localization of annexin A6 in Niemann-Pick type C human skin fibroblasts. Arch Biochem Biophys 493, 221–233.
Torrejon-Escribano B, Gomez de Aranda I, Blasi J (2002). SNARE expression and distribution during 3T3-L1 adipocyte differentiation. FEBS Lett 512, 275–281.

Umbrecht-Jenck E, Demais V, Calco V, Bailly Y, Bader MF, Chasserot-Golaz S (2010). S100A10-mediated translocation of annexin-A2 to SNARE proteins in adrenergic chromaffin cells undergoing exocytosis. Traffic 11, 958–971.

Urano Y, Watanabe H, Murphy SR, Shibuya Y, Geng Y, Peden AA, Chang CC, Chang TY (2008). Transport of LDL-derived cholesterol from the NPC1 compartment to the ER involves the trans-Golgi network and the SNARE protein complex. Proc Natl Acad Sci USA 105, 16513–16518.

Vila de Muga S *et al.* (2009). Annexin A6 inhibits Ras signalling in breast cancer cells. Oncogene 28, 363–377.

Wang P, Chintagari NR, Gou D, Su L, Liu L (2007). Physical and functional interactions of SNAP-23 with annexin A2. Am J Respir Cell Mol Biol 37, 467–476.

Wang Y, Thiele C, Huttner WB (2000). Cholesterol is required for the formation of regulated and constitutive secretory vesicles from the trans-Golgi network. Traffic 1, 952–962.

Wendler F, Tooze S (2001). Syntaxin 6: the promiscuous behaviour of a SNARE protein. Traffic 2, 606–611.

Wojtanik KM, Liscum L (2003). The transport of low density lipoprotein-derived cholesterol to the plasma membrane is defective in NPC1 cells. J Biol Chem 278, 14850–14856.